UNIVERSITÀ DEGLI STUDI DI PADOVA

Dipartimento di Fisica e Astronomia "Galileo Galilei"

Master Degree in Physics

Final Dissertation

Investigating the role of water in the protein dynamic transition

Thesis supervisor

Prof. Mario Bortolozzi

Thesis co-supervisor

Prof. Foivos Perakis

Candidate

Maddalena Bin

Academic Year 2019/2020

Abstract

Proteins undergo a dynamic transition at approximately 220 K, also called protein 'glass' transition, below which temperature proteins lose their conformational flexibility and become biologically inactive. The protein dynamic transition has been observed for several proteins utilizing different techniques, such as inelastic neutron scattering, infrared spectroscopy and X-ray crystallography. Water seems to play a role in this transition, especially in relation to the hydration layer surrounding the protein, termed hydration water, whose molecules interact with the protein surface. Despite various interpretations that have been advanced, the origin of the protein dynamic transition is still elusive.

Here, we investigate the protein 'glass' transition by means of infrared spectroscopy and X-ray diffraction, focusing on the enzyme lysozyme over the temperature range 160-295 K. Starting with the experimental implementation of the protein powder hydration setup, we study different levels of hydration of the protein, comparing them with the dry lysozyme as well as with protein solutions of different concentrations. We find a crossover in the lysozyme structure that occurs near 230 K, enhanced by the presence of hydration water.

Acknowledgments

I sincerely thank my supervisor Prof. Fivos Perakis from Stockholm University for his invaluable support and constant enthusiasm for the research during my Erasmus stay and later.

I also thank my supervisor Prof. Mario Bortolozzi for supporting my project and being always present.

I would also like to thank all XSoLaS group people of Stockholm University for being always available for advice and making me feel part of the group. In particular, I want to thank Rafat, Sharon and Sudipta for discussions throughout my project and for helping to carry out the XRD measurements. Moreover, I thank Alex and Katrin for the assistance in the laboratory, and Joakim, Egon, Gabriel, Marjorie and Jonatan for making me feel at home.

I owe a special thank to my university mates, Mattia, Federica, Giuseppe, Alessandro and Gianluca, for the countless hours spent together studying and drinking coffee.

I would also like to thank my family for the support during my studies and to always encourage me to broaden my horizons. Heartfelt thanks to Silvia, who has always been by my side despite the physical distance between us.

I acknowledge the Swedish Research Council for the financial support and Stockholm University, Heidelberg University and the University of Padova for giving me the opportunity to study around Europe with Erasmus+ program.

Indice

Nomenclature

LDL	Low-density liquid
HDL	High-density liquid
LLCP	Liquid-liquid critical point
PDB	Protein Data Bank
CS	Conformational substates
NAG	N-acetylglucosamine
NAM	N-acetylmuramic acid
QENS	Quasi-elastic neutron scattering
FSDC	Fragile-to-strong dynamic crossover
IR	Infrared
FT-IR	Fourier transform infrared spectrometer
XRD	X-ray diffraction
Ih	Hexagonal ice
DLS	Dynamic light scattering
XPCS	X-ray photon correlation spectroscopy
XFEL	X-ray free electron laser
TGA	Thermogravimetric analysis
SAXS	Small-angle X-ray scattering

Preface

Since ancient times, water has been acknowledged as the source of life and recognized, by philosophers like Aristotle and Socrates, as one of the four elements that constitute the nature of things, besides fire, earth and air. Water is an essential element of global issues of great importance to society, such as climate change, food production as well as its quality, availability and preservation. Indeed, *Clean water and sanitation* is the sixth of the 17 sustainable development goals devised by the United Nations to "*achieve a better and more sustainable world*" [53]. More precisely, the United Nations strives for clean and fresh water to be accessible for everyone, which is one of the most challenging goals for humankind.

Water's unique and fascinating properties have interested scientists for hundreds of years, however, the origin of its anomalies remains unclear. The understanding of the deepest mysteries of water is fundamental to address more complex systems, involving, for instance, biomolecules in aqueous environments.

During the last 30 years, the debate about the so-called protein 'glass' transition [47] has been an increasingly important area in the biophysics field, central for the knowledge of protein structure and dynamics. Water seems to play a significant role in the protein dynamic transition, concerning, in particular, the thin layer surrounding the solvated biomolecules, termed hydration water. Nevertheless, much uncertainty still exists in their relation. Resolving the origin of the protein 'glass' transition as well as its relation to hydration water is essential for understanding protein dynamics and functions. In the investigation of aqueous solutions, water is usually assumed as a passive solvent, disregarding its heterogeneities and structural peculiarities at a fundamental level. So how do these heterogeneities affect hydration and, more generally, the solutes?

For many proteins, the 'glass' transition occurs at 220 K [33], temperature at which hydration water can be supercooled and exhibits a different behavior than bulk water. Furthermore, confining water at the thin layer of hydration surrounding biological molecules is a possible method to get access to the metastable supercooled region of water, the so-called 'no man's land' [25].

The study of aqueous systems at cool temperatures has many applications that are beneficial for society. One example is the cryopreservation of biological animal or vegetable material, which is the use of very low temperatures for the preservation of living organism structures and functions over time [7]. Cryosurgery [37] is a second important application in medicine, used to destroy pathogenic organisms in cancer treatment, for instance. Therefore, deeper comprehension of water and protein systems will certainly lead to find new applications and benefits in the field of medicine as well as in physics, biology and chemistry at a fundamental level.

The aim of this work is to investigate the role of water in the protein dynamic transition by means of two techniques, infrared spectroscopy and X-ray diffraction, focusing on the enzyme lysozyme across a temperature range from T=295 K to T=160 K. The former technique probes the vibrational modes of molecules, such as the stretching and bending modes of OH bonds in water molecules, and general information about the dynamics. The latter method examine the structure of the compounds analyzed. The samples probed include dry and hydrated lysozyme powder with variable humidity levels measured over a broad temperature range as well as aqueous solutions of different concentrations.

Regarding X-ray measurements, we observe a shift of the intensity in the hydrated lysozyme powder with respect to dry powder and a crossover in the lysozyme structure that occurs near 230 K. This crossover is enhanced by the presence of hydration water.

The work is arranged as follows:

Chapter 1 Introduction of the topic with a review of the existing studies.
Chapter 2 Materials and methods utilized in the present work.
Chapter 3 Discussion of the results obtained.
Chapter 4 Conclusions of the work and future outlook concerning the investigation of the protein dynamic transition.
Appendix A Tables reporting infrared bands of water and protein vibrational modes.
Appendix B Experimental setup employed for infrared spectroscopy, X-ray diffraction and hydration of protein powder.
Appendix C Additional plots of the measurements done.
Appendix D Tables with raw data.

Capitolo 1

Background

In this chapter we present the two building blocks of our investigation giving a general introduction: water and proteins. Next, we outline an overview of the debate among the scientific community on the protein dynamic transition and we summarize the main hypotheses that emerge from the research and studies which have been done so far.

1.1 Water: anomalies and a hypothesized model

Water exists naturally in the three physical states over a relatively narrow temperature range: solid, liquid and vapor [18]. It plays and essential role in many subjects, including physics, chemistry and biology. Its well-known phase diagram (P,V,T) describes the features and underlines the anomalies of this liquid, such as the increased density on melting and the density maximum that occurs at 4°C under ambient conditions. This peculiar behavior of water allowed the development of life in oceans and seas during the cold seasons. An additional characteristic is its large heat capacity, which helps living organisms to thermally self-regulate more easily. Further, thanks to the heat capacity, oceans and seas act as reservoirs for the Earth, preventing our planet from reaching extreme temperatures. Life has developed on Earth thanks to these and many other anomalies of water [31] [4], justified by the tetrahedral hydrogen bond network. However, the exact physical relation between water structure and its properties remains elusive.

Despite having been studied for several centuries, water still hides many mysteries. For instance, in the region between the temperature of homogeneous nucleation $\mathrm{T}_X = 231\,\mathrm{K}$ and $\mathrm{T}_H \sim 150\,\mathrm{K}$, below which water becomes a highly viscous fluid, metastable supercooled water is located and has not been completely studied since it is not experimentally accessible for bulk water [14]. The reason is that rapid ice crystallization occurs preventing water to be probed. The region we are talking about is the so-called 'no man's land', depicted in the phase diagram of figure 1.1a.

Although probing water in the no man's land is experimentally arduous, it was demonstrated that it can be investigated through experiments based on fast supercooling utilizing X-ray lasers on water droplets [25] [49]. Confined liquid water is another approach to investigate the metastable supercooled state of water, which can also be done by exploiting thin water layers surrounding biomolecules [16], as will further discussed in section 1.3.

One popular hypothesis to explain the 'no man's land' attributes two liquid phases to water: a low-density liquid (LDL) and a high-density liquid (HDL). Between these two states, there is a phase coexistence line which ends to a second order liquid-liquid critical point (LLCP) [44], shown is figure 1.1b. Beyond the critical point, the two liquid phases are no longer separated. They are replaced by a one-phase region where one phase dominates with respect to the second one. In other words, this phase is a mixture of fluctuating local structures, appearing and disappearing, immersed in a dominant phase.

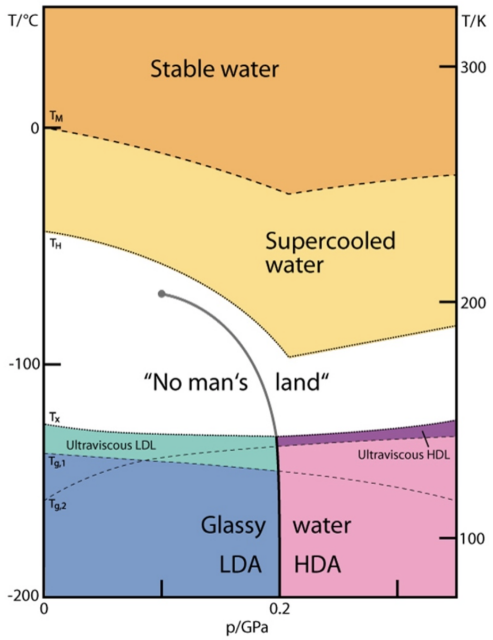

(a) Water phase diagram (T,P) showing the supercooled liquid water region and the metastable supercooled region, namely 'no man's land', with the hypothesized liquid-liquid coexistence line ending in the liquid-liquid critical point [27].

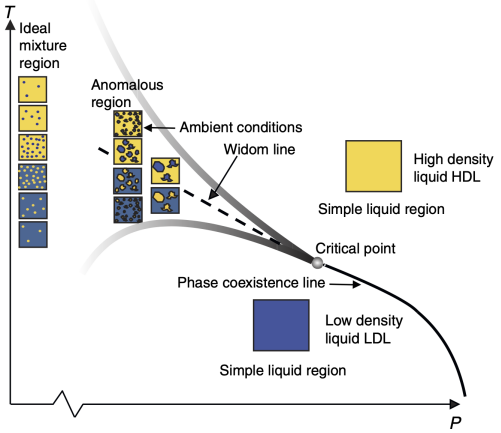

(b) Schematic of the hypothesized liquid water phase diagram (T,P) showing the liquid-liquid coexistence line between low- and high-density liquid phases ending in the liquid-liquid critical point. The local fluctuations of the one-liquid phase are depicted in the anomalous region between the gray lines as they cross the Widom line [38].

Figura 1.1: Water phase diagrams describing the hypothesized low-density and high-density liquid phases.

Therefore, above the phase coexistence line, the region is described as a high-density liquid with small islands of the low-density region. The opposite below the phase coexistence line, where liquid water is of the low-density type with local areas of high-density liquid. Going from one region where one liquid is dominating to the region where the other liquid is predominant, a line is crossed. This curve is what we refer to as the Widom line, which is an extension of the liquid-liquid coexistence line. The Widom line was recently observed experimentally for deeply supercooled water [25].

The continuous fluctuations between LDL and HDL would explain the anomalous properties of liquid water. In the last years, relevant progress has been done, however several open questions remain to be answered. For instance, what is the interplay between

water and solutes taking into consideration water heterogeneities? What is the influence of water in the structure and dynamics of molecules essential for the development of life?

1.1.1 The water molecule and the hydrogen bond

From a geometrical point of view, the water molecule is characterized by two O–H bonds of $\sim 1\,\text{Å}$ length which form an angle H–O–H of 104° at equilibrium. The molecule is constantly vibrating and rotating, depending on the thermal energy available, giving rise to vibrational modes. The main vibrational modes are symmetric stretch (ν_1), bend (ν_2) and antisymmetric stretch (ν_3) depicted in figure 1.2a. As well as stretching and bending modes, water molecules are also characterized by librations (L_1, L_2, L_3), namely rotations of the solid molecule with respect to one axis. The water infrared vibrational frequencies of the water molecule in the liquid phase are reported in table A.1 of appendix A. The infrared spectrum with water vibrational modes will be further discussed in chapter 3.

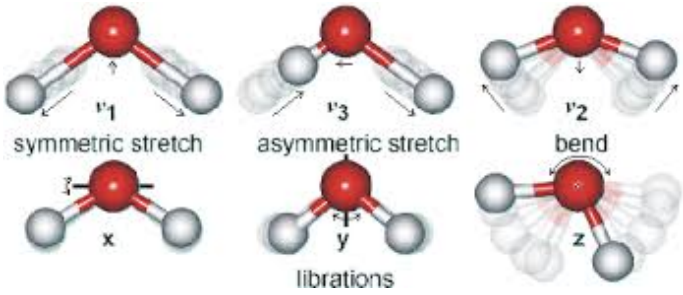

(a) Water molecule vibrational modes: OH-stretching (ν_1, ν_3), OH-bending mode (ν_2) and librations (L_1, L_2, L_3) [31].

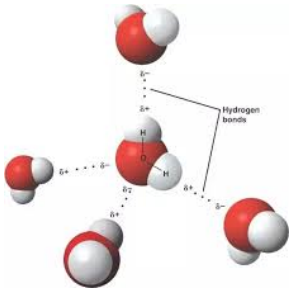

(b) Water tetrahedral structure maintained by hydrogen bonds connecting oxygen to hydrogen atom belonging to different molecules.

Figura 1.2: Water vibrational modes and tetrahedral structure with hydron bonds.

In the water molecule, the oxygen nucleus attracts electrons more than hydrogens, as its electronegativity is higher due to the nucleus positive charge ($E_{oxygen} = 3.44$, $E_{hydrogen} = 2.20$ according to the Pauling scale). Hence, the water molecule is a dipole with a partial positive charge located in the hydrogen side, usually termed δ_+, and a partial negative charge δ_- on the oxygen side. This is the basis of the hydrogen bond that is formed between hydrogen and oxygen atoms belonging to different molecules. Each water molecule can form 4 hydrogen bonds, two involving the hydrogen atoms and two involving the oxygen atom. Water molecules bound by means of hydrogen bonds arrange themselves tetrahedrally, as displayed in figure 1.2b. This structure is stable in crystalline ice, also called hexagonal ice (Ih), while in liquid water the thermal energy stretches and bends the hydrogen bonds, and sometimes even breaks them. The hydrogen bond is always weaker than the covalent OH bond, however, it is strong enough to maintain during thermal fluctuations at room temperature. Its short lifetime is estimated to be approximately 1 ps with a length of $0.238 - 0.3\,\text{nm}$ [18].

1.2 Proteins: general introduction on their structure and energy landscape

Proteins are among the most important biological molecules. Indeed, the majority of living systems is made up of proteins. They conduct an incredible variety of different functions essential for the development of organisms. As an example, a human cell contains about 18,000 different types of proteins, each of them with an assigned role [3]. They are biomolecules consisting of amino acid chains, which are identified as the fundamental units of proteins and there exist mainly 20 different types. The molecule formed by many amino acids is in general termed polypeptide. Amino acids are made of carbon (C), hydrogen (H), oxygen (O) and nitrogen atoms (N). The basic structure of each amino acid has a central carbon bound to an amine group ($-NH_2$), to a carboxylic group ($-COOH$) and to a hydrogen atom. The amino acids differ in the fourth covalent bond of the central carbon atom. The three-dimensional stable structure of proteins under normal conditions is called native or folded configuration. The structures of all known proteins are collected in the Protein Data Bank (PDB) [5]. However, proteins are not always found in their native state. Under certain conditions, proteins can denaturate, namely unfold, becoming linear polypeptide chains and losing their three-dimensional structure (figure 1.3a). This causes the loss of functionalities and anomalies in protein behavior. For instance, the misfolding, i.e. folding failure, seems to have enormous consequences as the development of diseases such as cystic fibrosis, Alzheimer's and Huntington's [3].

Each protein is identified by its unique amino acid sequence, the primary structure, that determines all chemical and biological properties [11]. As well as the primary structure, additional three hierarchical levels and structures constitute proteins, as displayed in figure 1.3b. The secondary structure arises from the local conformation of the amino acid chains and can be of two different types: α helices and β sheets, distinct into β strands and β turns. Their characteristic structure is maintained by hydrogen bonds. Moreover, the complex tertiary structure is formed by folded secondary structures. Finally, the assembly of many chains makes up the quaternary structure. Hemoglobin, the protein found in red blood cells responsible for the oxygen transport through the body, is an example of a protein containing the quaternary structure.

Proteins can assume a wide variety of conformations moving between different free energy levels. The characterization of free energy levels is therefore a key point for understanding protein motion and dynamics. In general, each proteins has different structures, meaning that its energy landscape has valleys, each corresponding to a macrostate (cs^o), as displayed in figure 1.4.

Looking closely at one of the energy minima, we will discover a large number of microstates, which are called *conformational substates* (CS) [20]. Each of these microstates has in turn different conformational substates, giving a hierarchical organization featured by different tiers. As an example, we report the case of myoglobin [21], which is a globular protein whose function is to reversibly bound oxygen. Myoglobin has two macrostates, bound and unbound. Taking into account the bound state and "zooming" into its corresponding minimum in the free energy landscape, we find a rough structure of small substates (cs^1), identifiable with stretching bands. In other words, the substates correspond to a protein state with the same amino acid chains but with different geometry of the bonds. Furthermore, energy barriers with different heights divide the conformational

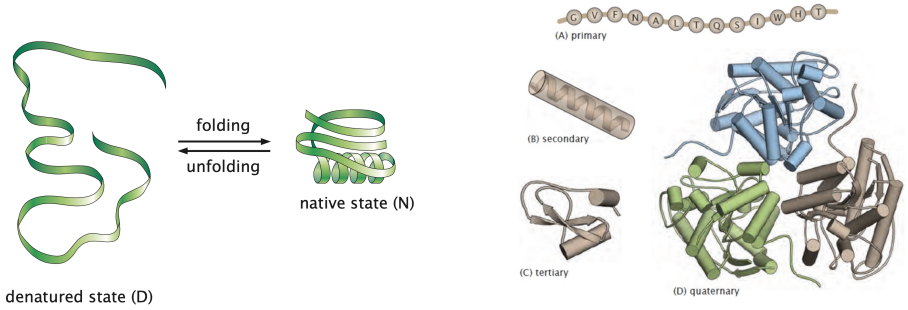

(a) Schematic of protein native and denaturated states.

(b) Illustration of the protein hierarchical structure: primary (peptide chain), secondary (α helix and β sheet), tertiary (folded secondary structure) and quaternary structures (assembly of chains).

Figura 1.3: Protein states and structure. [3]

substates. The protein can jump from one state to another, crossing the energy barriers, according to the energy available, and thus giving a certain motion.

From a theoretical point of view, the protein free energy landscape with its conformational substates can be studied by connecting it to a comparable system with a rugged energy landscape. The comparable system is spin glass model [6]. Its statistical approach is needed for lower tiers, as the level of complexity is too high for a mechanical study. From an experimental point of view, on the other hand, to investigate transitions between different states, one might examine spectral lines at different wavelengths. Spectral lines are broad for complex systems, such as proteins, and sometimes very difficult to interpret.

Proteins are dynamic systems, thus they repeatedly leap from one state to another, exploring the free energy landscape. This motion is strongly related to the temperature of the system. At lower temperatures, any given molecule will stay in a certain conformational substate, whereas at room temperature it will frequently jump to new substates. As a general rule, there are two types of motion: relaxation processes and equilibrium fluctuations. In the former, the system goes to an equilibrium state starting from a non-equilibrium one. It is a collective phenomenon and it might occur even for a single protein, because of the large number of constituents, namely bound atoms. The latter is a type of motion that occurs within an equilibrium state, in which the system hops from one conformational state to another. Among the relaxation processes, we identify α relaxation, namely large-scale motions, such as the first tiers of the energy landscape (cs^1), and β relaxation, that is relevant for lower tiers (cs^2, cs^3,...) and involves the motion of local regions of the system [23].

1.2.1 Lysozyme

Lysozyme is a hydrolytic enzyme discovered in 1922 by Alexander Fleming [17] and depicted in figure 1.5. Its biological function is to destroy bacteria by hydrolysis, a chemical reaction in which molecules are divided into two or more parts by means of water. Water penetrates into the bacterium after lysozyme breaks its bonds, causing the lysis of the

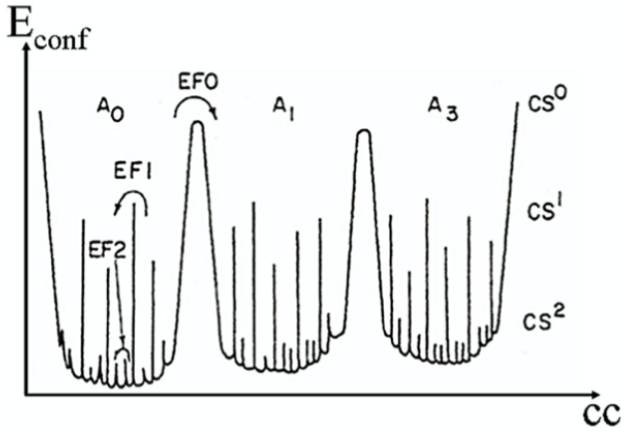

Figura 1.4: The rugged protein free energy landscape showing the tiers ($cs^0, cs^1, cs^1, \dots$) representing the different conformational states [19].

bacterium. More specifically, the lysozyme active site breaks the glycosidic bonds between N-acetylglucosamine (NAG) and N-acetylmuramic acid (NAM), two monosaccharides contained in the polysaccharide components of cell walls. In addition, lysozyme hydrolyses also poly-NAG chains contained for example in fungal cell walls.

Hence, lysozyme is the guardian of our body. It is made of 129 amino acids and has an elliptical shape (3.0 x 3.0 x 4.5 nm), which was first determined by David Phillips in 1965 by means of X-ray crystallography [43], and it features an active site, like a pocket, which breaks bacteria walls. Lysozyme contains five α helices and one β-sheets formed by three β strands. The optimum pH for lysozyme is 5.0 [55]. Lysozyme is found in animal and human secretions, such as tears, egg white, saliva and human milk. Nowadays, lysozyme is exploited as a preservative in the food industry.

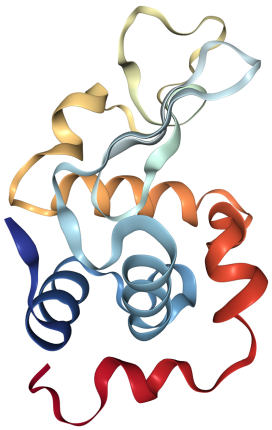

Figura 1.5: Lysozyme structure showing α helices and β sheets.

1.3 The protein dynamic transition

In the previous sections, we introduced the two ingredients of this investigation, water and proteins, underlining their structures and describing the properties and behaviors that we will consider in the following discussion. Now, we want to explore in detail the connection of water to the protein dynamic transition [47].

The interaction between water and solvated biomolecules, such as proteins, is often described considering the so-called hydration water, which is a water layer within the first few solvation layers. Hydration water seems to play a role in the dynamic transition, also called protein 'glass' transition, of biomolecules, such as proteins, DNA and RNA [8]. The reason why the transition is termed as 'glass' transition is that the protein transition resembles the change of the viscosity and other properties of liquids when they form a glass.

It was observed that proteins exist in a 'glassy' state [2] below their transition temperature, which is near 220 K for many proteins [15]. When they are in the glassy state, proteins show no conformational flexibility and the predominant behavior is characterized by harmonic vibrations of atoms [30]. In this state, they lose biological functions. Above the transition temperature, the protein is able to leap between different conformational substates returning to its original functions and flexibility. As a result, it becomes biologically active and the dynamic behavior features collective motions of bonded groups of atoms.

Furthermore, proteins need water to execute their biological functions. Indeed, they live in aqueous environments, like our body, where they can conduct the functions they are made for. Dry proteins are not active [10] [57], but a single layer surrounding the protein restores their functionality. In order to quantify the amount of hydration, we introduce the hydration level h, defined as the ratio of water and protein masses:

$$h = \frac{m_{\text{water}}}{m_{\text{protein}}} \tag{1.1}$$

For instance, $h = 0$ corresponds to dry protein as the water mass is zero, while $h = 1$ describes a compound made of water and protein in equal parts. According to Rupley and Careri, a hydration value of $h \approx 0.3$ is the amount of water needed to have a monolayer that completely covers the protein [48], which corresponds to 0.3 g of water per gram of protein. It was observed that, in the case of lysozyme, the biochemical activity was very low up to $h = 0.2$. Whereas, going from a hydration level of $h = 0.2$ to $h = 0.5$, the protein activity was enhanced. Both experiments and computer simulations proved the influence of the hydration level on protein dynamics [24] [28]. Therefore, the knowledge of the behavior of hydration water is of utmost importance for understanding how it affects the conformation and dynamics of proteins.

Water molecules interacting with proteins are usually classified into three categories: internal water, hydration water and bulk water. Internal water corresponds to bound water molecules placed in protein cavities and clefts and they play a primary role in the folding and unfolding processes, thus being relevant for protein structure. Hydration water molecules are part of the water layer surrounding the protein and interacting with its surface atoms. Lastly, water molecules that do not directly interact with the protein surface are commonly refer to as bulk water.

The investigation of the protein dynamic transition started about 30 years ago studying how the protein motion and functionality are affected by the temperature, when scientists discovered that protein motions are not all sensible to temperature in the same way [47]. In the last decades, different proteins have been studied, such as myoglobin [15], ribonuclease A [46] and lysozyme [34], by means of different techniques, including inelastic neutron scattering [15], X-ray crystallography [46], quasi-elastic neutron scattering [9] and dielectric spectroscopy [40]. The literature on the protein dynamic transition is rich and relevant progress has been done during the last years. However, the origin of the transition divides the scientific community and different views propose different explanations. Summarizing the different hypotheses, one view proposes that the solvent does not play any relevant role in the dynamic crossover observed in the protein dynamic transition [29]. A second view, instead, proposes that the solvent does play a role in the protein 'glass' transition, but the mechanism at the origin is still debated [54]. Assuming that the protein glass transition is driven by water, what are the mechanisms whereby water gives rise to it?

Previous experiments and simulations highlight that hydrated proteins undergo a glass transition at 220 K. Therefore, a key point is to understand the role of hydration water on the dynamical transition. It is worth noting that confined water can be experimentally supercooled to temperatures not accessible with bulk water [16], and this is the case of the hydration water, which is exploited also to obtain more information on the water metastable supercooled phase.

It was observed that, when a protein is hydrated, the protein glass transition is strongly coupled to the solvent. Additionally, it has been demonstrated that the dynamic transition can be suppressed in dry biopolymers [10] and that the transition temperature changes for proteins dissolved in a different solvent [52]. Hence, the solvent plays a crucial role in the protein dynamic transition. However, it is still debated whether the dynamic transition is directly related to the dynamic transition of the surrounding solvent or not.

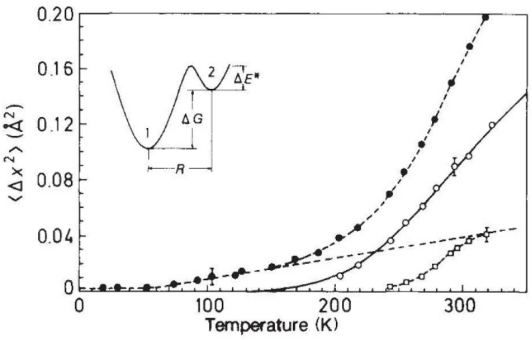

Figura 1.6: Results obtained by inelastic neutron scattering probing myoglobin. The plot shows the mean-square displacement of hydrogen atoms as a function of temperature. The dashed straight line describes the harmonic dynamics with only vibrations extrapolated from low temperature behavior [15].

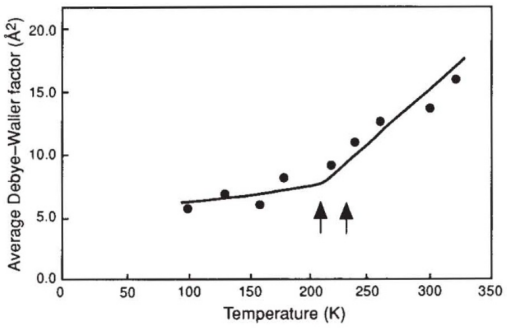

Figura 1.7: Results obtained by X-ray diffraction on ribonuclease A. The plot reports the Debye-Waller factor for the non-hydrogen protein atoms as the temperature varies. It shows a slope change near 220 K [46].

Experiments on hydrated myoglobin carried out employing inelastic neutron scattering over a temperature range of 4-350 K and on molecular dynamics timescale 0.1-100 ps were performed in 1989 by Doster et al [15]. The method analyzes the motion of hydrogen atoms giving a general view of the protein dynamics, as hydrogens are abundant both in the protein and hydration water. Doster et al. observed that below 180 K the protein behaves as harmonic solids with only vibrations (figure 1.6). Whereas, above 180 K there is an abrupt dynamic transition, which they interpret to arise from jumps between states of different energy causing non-vibrational motion. Figure 1.6 shows the mean-squared displacement of hydrogens at different temperatures. The dashed line represents only vibrational modes and it is extrapolated from the low temperature behavior. From 180 K there is a clear increasing deviation from the only vibrational behavior in the dynamics of myoglobin. In this experiment the protein is considered as a solid, not taking into account its microscopic structure. They read the protein dynamic transition as a coupling between fast local and slow collective motions, therefore related to the protein free energy landscape.

In 1992 Rasmussen et al. investigate the dynamic transition of crystalline ribonuclease A by means of X-ray diffraction [46]. In figure 1.7 they show the average Debye-Waller factor as a function of temperature. The Debye-Waller factor is used to describe the attenuation of X-ray scattering due to thermal motion and it reflects the amplitude of the vibrations of different parts of the protein. The Debye-Waller factor decreases as the magnitude of the reciprocal lattice vector $\vec{G}$ increases, at a given temperature [26]. The temperature transition is estimated to be approximately 220 K. Here they demonstrate that the dynamic crossover happens, not only for protein powder, but also for crystals.

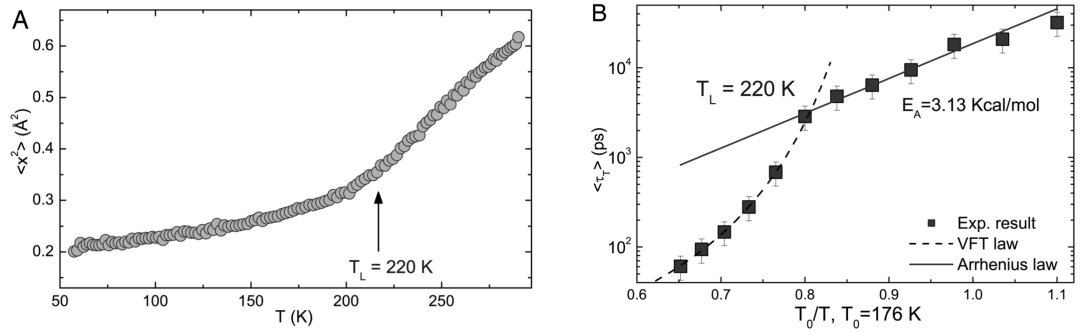

(a) Mean-square displacement of hydrogen atoms as a function of temperature. A change of the slope is found near 220 K.

(b) Average translational relaxation time as a function of temperature. A crossover from a Vogel–Fulcher–Tammann law at high temperatures to Arrhenius law at low temperatures is clear at 220 K.

Figura 1.8: Experimental evidence of the protein 'glass' transition obtained by quasi-elastic neutron scattering on lysozyme [9].

Experiments on lysozyme utilizing quasi-elastic neutron scattering (QENS) made by Chen et al. in 2006 [9] point out that the dynamic transition of hydration water reflects the fragile-to-strong dynamic crossover (FSDC) at T = 220 K (figure 1.8), temperature which is in agreement with Rassmussen et al. [46]. They highlight the dynamic transition plotting the temperature dependence of the mean-squared atomic displacement figure 1.8a

of hydrogen atoms. At 220 K the plot shows an abrupt change in the slope of the curves. Furthermore, figure 1.8b presents the temperature dependence of the average translational relaxation times of hydrogen atoms. At low temperatures, the translational degrees of freedom follows a typical Arrhenius behavior, signature of a strong liquid, which means there is a single activation barrier in the free energy landscape. Whereas, at higher temperatures, a transition to a Vogel-Fulcher-Tammann law happens [1], signature of a fragile liquid. It indicates multiple activation barriers in the free energy landscape of the hydration water.

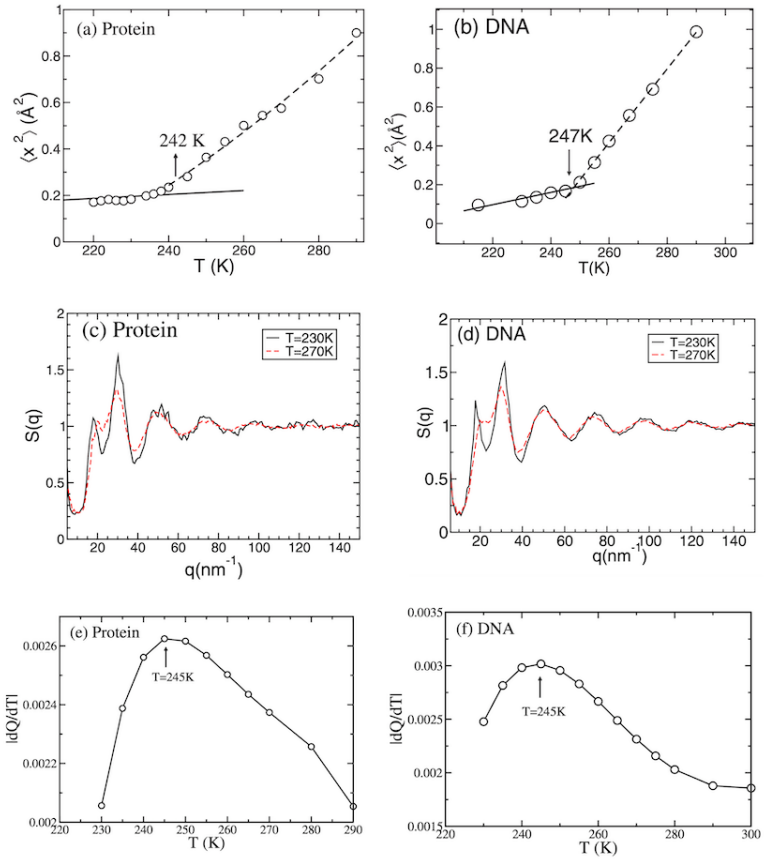

Figura 1.9: Molecular dynamics simulations of lysozyme and DNA. Mean-square fluctuations of lysozyme (a) and DNA (b) as a function of temperature showing a slope change near 240 K. Structure factor as a function of the momentum transfer of hydration water surrounding lysozyme (c) and DNA (d) at two temperatures (230, 270 K). The line corresponding the behavior at lower temperature shows sharper peaks meaning that water is more structured at that temperature; they refer it to the low-density liquid phase of water. The derivative of the order parameter Q with respect to the temperature is plotted for lysozyme (e) and DNA (f) showing a maximum at 245 K, temperature at which the Widom line is hypotesized to be [28].

In the same year, Kumar et al. [28], utilizing molecular dynamics simulations, investigated the relation between the glass transition of lysozyme and DNA and the dynamic and thermodynamic properties of hydration water. In figure 1.9a,b they observe a tran-

sition looking at the mean square fluctuation of lysozyme and DNA as the temperature varies, similarly to Doster et al. [15], and at the diffusion constant of hydration water surrounding these two biomolecules. Unlike Doster et el., they relate the crossover to the high-density and low-density liquid water. This is explained by looking at the structure factor of hydration water surrounding lysozyme and DNA (figure 1.9c,d) at different temperatures. The first peak appears to be sharper at low temperatures, reflecting the more open tetrahedral hydrogen bond network structures of the low-density liquid with respect to the high-density liquid. Taking the derivative of the local order parameter Q with respect to temperature (figure 1.9e,f), a maximum appears at 245 K, the temperature where the Widom line for water is expected.

They conclude that the glass transition occurs at the same temperature as the dynamic crossover in the diffusivity of hydration water. In addition, the crossover in the diffusivity of hydration water corresponds to the maximum of the temperature derivative of the order parameter. They read this result as related to the crossing of the Widom line by the hydration water, assuming that the hypothesized liquid-liquid critical point exists.

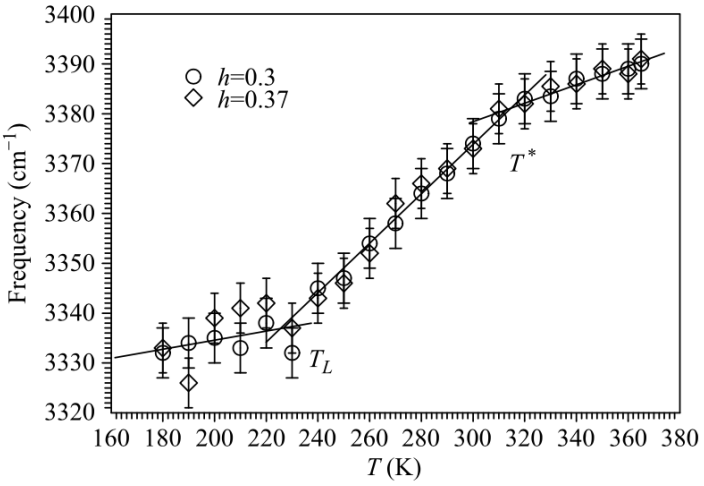

Figura 1.10: Infrared spectroscopy of hydrated lysozyme, showing the OH-stretching mode peak centers as the temperature changes. Two crossovers are evident observed as slope changes: at $T_L \sim 220\,K$ the protein dynamic transition and at $T^* \sim 315\,K$ the transition from the native to the denaturated structure [34].

More recently, Mallamace et al. report the frequency of OH-stretching mode as the temperature varies from 180 K to 365 K measured with Fourier transform infrared spectroscopy on hydrated lysozyme [34]. Figure 1.10 shows two evident crossovers: the first at $T_L \sim 220$ K is the protein dynamic transition we are interested in, and the second at $T^* \sim 315$ K is a transition related to the denaturation temperature of lysozyme. This second crossover is believed to be the transition of the protein from its native to its denaturated state, which become an irreversible transition at 350 K. Mallamace and coworkers explain the protein dynamic transition as affected by the strong coupling between the protein and hydration water due to hydrogen bonding. The strength of hydrogen bonds influences the OH stretching vibrations, suggesting that the polymorphism of glassy water and the hydrogen bond network might imply that water exists in two different liquid

states, the already mentioned low-density and high-density liquids.

Many investigations employing different techniques, studying several proteins utilizing diverse preparation procedures have been done so far. Another issue is that the different techniques utilized are sensitive to several aspects of the hydrated protein system, being not straightforward to compare them. As a result, the protein dynamic transition remains debated among the researchers.

1.3.1 Hypotheses

These studies clearly indicate that the relationship between hydration water and the protein dynamic transition is not clear. Two important themes emerge from the studies discussed so far: either water plays a role or it does not. Assuming that water does play a role opens, in turn, two positions: the origin of the dynamic crossover is caused by the water free energy landscape (fragile-to-strong dynamic crossover) or by the two liquid phases of water (low- and high-density liquid phases). Here, we summarize these three hypotheses.

Water does not play a role: protein energy landscape In section 1.2 the protein energy landscape was described. We recall that its roughness is related to different conformations states, such as bound or unbound states, but also to vibrational or rotational modes associated to lower tiers. Within this framework, the first hypothesis states that the 'glass' transition has to do with protein degrees of freedom. Going below the critical temperature T_c, protein behaves resembling harmonic solids, so it is in a macroscopic state with no enough energy to leap to another state. In this manner, it loses its conformational flexibility and is not active anymore, not executing its biological functions. On the other hand, above the critical temperature the protein can jump from one state the other, being in this way active. The activity is due to the coupling between fast and slow collective degrees of freedom. Referring to the free energy landscape description given, this first hypothesis states that protein glass transition is related to the protein energy landscape and the coupling between faster and slower modes belonging to different tiers of the protein free energy landscape. Another possibility is that the observed behavior is due to the cold denaturation of the protein.

Water plays a role: water energy landscape The protein glass transition is caused by the water around the protein, namely hydration water, that experiences a change in its free energy landscape. Conversely the first hypothesis, the protein dynamic crossover is related to the free energy landscape of the solvent, specifically water. Below the critical temperature, water behaves like a strong glass former [13] associated to a sharp minimum in the energy landscape, as depicted in the top part of figure 1.11a. If there is only a single minimum, it means a single structure in the hydrogen bond network exists, which is the stable conformation, and the energy available is not enough to leap to another state. On the other hand, above the critical temperature, water behaves like a fragile substance, which means there are several minima in the free energy landscape (bottom part of figure 1.11a), thus many stable conformations for water structures. In this case, the protein glass transition is triggered by the fragile-to-strong dynamic crossover (FSDC) of the hydration water, related to the water free energy landscape. The strong and fragile

pattern of substances is well described by the so-called Angell's plot, shown is figure 1.11b. It shows the liquid viscosity as a function of the inverse temperature. Strong liquids exhibit linear dependence, i.e. Arrhenius behavior with a single activation energy barrier, while fragile liquids display super-Arrhenius behavior with multiple basins in the energy landscape. Glass formers either follow one behavior or the other or both, like water [50]. From this point of view, water is believed to behave like a fragile glass former at room temperature but resembling the behavior of strong glass formers towards colder temperatures.

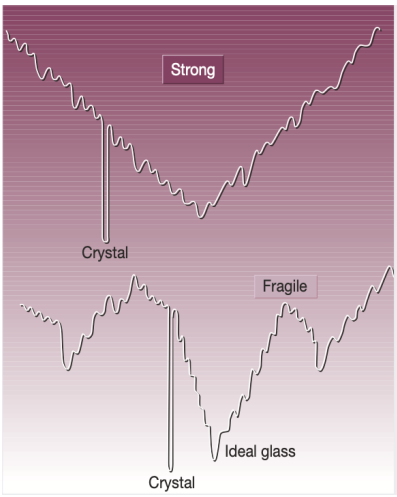

(a) Free energy landscape of fragile (bottom) and strong (top) substances. In the y axis the energy increases vertically and the x axis represents the collective coordinates [13].

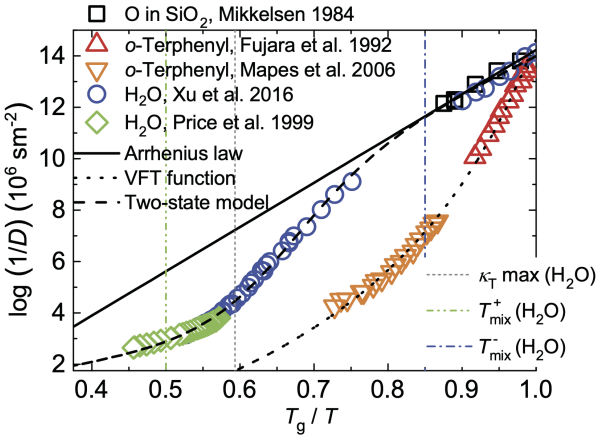

(b) Angell's plot for water showing the inverse diffusivity logarithm as a function of the inverse temperature. The straight line represents the Arrhenius behavior of strong liquids while the dashed line represents a multi-basin free energy landscape of fragile liquids [50].

Figura 1.11: Strong and fragile liquids energy landscape of substanced (a) and Angell's plot for water (b).

Water plays a role: Widom line The protein 'glass' transition is driven by water's 'glass' transition interpreted as the liquid-liquid phase transition. Above the critical temperature, water is dominated by high-density liquid with small islands of low-density liquid. Crossing over the Widom line, the predominance of HDL with local LDL islands transforms to a more relevant contribution of LDL with local HDL regions (figure. 1.1b). Within this framework, the protein crossover reflects the change in the water structure when crossing the Widom line.

Capitolo 2

Method

In this chapter we illustrate the methods utilized to investigate the role of water in the protein dynamic transition. The study was carried out by means of Fourier transform infrared spectroscopy and X-ray diffraction. The former is an analytical technique used to obtain the vibrational spectrum of a certain material, including liquids, solids and gases in the infrared electromagnetic spectrum. The latter is a useful technique to investigate the structure of the material of interest.

2.1 Fourier transform infrared spectroscopy

Fourier transform infrared spectroscopy (FT-IR) is a technique used to characterize the dynamics of the compounds of interest measuring their vibrational spectra, that is the absorption or transmittance. Infrared spectroscopy is a technique widely employed for scientific purposes thanks to its relatively inexpensive cost and to its simplicity of use. This method indirectly probes the dynamics of the molecules at a broad timescale of motion of 10 ps - 10 fs [42].

The molecules of the sample interact with the incident electromagnetic field absorbing a part of the radiation. The incident radiation with intensity I_0 goes through a medium of thickness x, a part of this radiation is transmitted with residual intensity $I(x)$. The relation between the incident and outgoing radiation intensities is given by

$$I(x) = I_0\, e^{-\alpha x} \tag{2.1}$$

where α is the absorbance coefficient, which is a specific constant for the medium crossed and the wavelength of the incident electromagnetic wave. In order to calculate the amount of radiation transmitted, we defined the transmittance T as

$$T = \frac{I}{I_0} = 10^{-A} \tag{2.2}$$

where I_0 and I are the incident and transmitted intensities respectively, and A is the absorbance, which quantifies the absorbed radiation. Rearranging this equations one obtains

$$A = -\log\left(\frac{I}{I_0}\right). \tag{2.3}$$

In the case of liquid samples, an additional definition of the absorbance is the so-called Lambert-Beer equation

$$A = \epsilon\, c\, d \tag{2.4}$$

where ϵ is the extinction coefficient and it determines the optical absorbance of the electromagnetic wave, related to the absorbance coefficient α, c is the concentration of the solution and d is the thickness of the sample.

2.1.1 Experimental setup

The experimental setup consists of four parts: IR spectrometer, cryostat, vacuum pump and temperature controller.

The Fourier transform infrared spectrometer used was Frontier MIR/FIR by Perkin Elmer. It allows measuring either absorbance or transmittance spectrum of a certain sample in the frequency interval of $8300 - 350\ \mathrm{cm}^{-1}$. This range is commonly referred as near-IR and mid-IR.

The cryostat VPF-100 Optical Cryostat manufactured by Janis Research Company, LLC was used to keep the samples in a vacuum environment and at variable temperatures. The vacuum shroud of the cryostat is connected to a manually controlled oil-sealed vacuum pump, manufactured by Low2High Vacuum, in order to minimize the noise due to air and avoid ice building on the sample when the measurements were carried out at low temperatures. The vacuum accessible in the vacuum compartment with the instruments was about $(5 \pm 0.5) \cdot 10^{-3}\,\mathrm{mbar}$, read with a pressure gauge (digital Thermovac TM 101); this level of vacuum was achievable only when all the connections were clean and greased with vacuum grease. For the cooling, the cryostat reservoir was filled with liquid nitrogen, whose boiling point is at 78 K, through a displacer assembly. The temperature was electronically controlled by a temperature controller Model 335 manufactured by Lake Shore Cryotronics, Inc. It is possible to control it via computer interface using a software that permits to log the temperature as a function of time, useful to check the thermal stability while taking measurements. It was connected to a heater placed on the sample mount made of copper at the extremity of the cryostat in thermal contact with the optical sample holder. Two sample holders were available based on the size of the windows.

The samples are prepared on circular Calcium Fluoride (CaF_2) windows provided by Crystran Limited, and fixed on the sample holder with four screws. CaF_2 is an inorganic compound, suitable for the experiment as it is transparent in the frequency range of interest, that is $\bar{\nu} \in [1000 - 6000]\,\mathrm{cm}^{-1}$. The thickness of the windows was 2 mm and we tested two different diameters of 10 and 20 mm.

The lysozyme protein used is lyophilized powder from chicken egg white purchased by Sigma-Aldrich.

2.1.2 Sample preparation

A key task of this thesis was to implement a protocol for the preparation of liquid samples, as protein solutions, powder samples, like dry protein powder and, more importantly, hydrated protein powder.

All samples measured in the FT-IR were prepared on CaF_2 windows. In the case of liquid samples, such as water or lysozyme solutions, a small droplet of about $2\,\mu\mathrm{l}$ was

placed on the face of a CaF_2 window. Then, a second window is placed on top of the first, so that the droplet is spread into a thin layer. The thickness of the sample is proportional to the absorbance, as expressed by equation 2.4, and it is important, in order to avoid any saturation effects, to press the windows in order to get a thinner layer of the liquid sample. Before starting the sample preparation, it is essential to carefully clean the windows to dispense with impurities and avoid any contamination. The solutions are prepared by weighting the exact amount of grinded lysozyme powder necessary for the solution and adding the needed amount of Milli-Q water [56].

In the case of powder samples, a small amount of protein powder, less than $1\,mm^3$, was placed on the face of a window. The powder was previously grinded with a mortar to reduce the particle size, but was not further dried. Then, the powder is spread swiping a second window. In this way, it is possible to obtain a thinner layer of protein powder. The last step consists in placing a second clean window on top of the first one.

The setup used for preparing the hydrated protein powders is depicted in figure 2.1, built in order to control the humidity level inside the chamber. Nitrogen gas with a pressure of $\sim 1.5 - 2\,bar$ flows in a glass bottle filled with pure water, heated up by Peltier elements. In this way, water molecules are facilitated to travel through a tube, which leads to a closed chamber. The chamber is the top part of MultiTherm Shaker H5000-HC produced by Benchmark Scientific, Inc. This instrument allows to control the temperature of the chamber and, when needed, to shake it so that the samples were more homogeneously hydrated. A small amount of lysozyme powder, less than $1\,mm^3$ of volume, was spread on one window in order to have a thin layer, as in the case of powder sample preparation. Next, the window was placed in the chamber set at 5°C and exposed to water vapor. The humidity level was controlled by the concurrence of different parameters, such as the nitrogen gas pressure, the Peltier and chamber temperatures. The conditions we used allowed us to get ∼70% of relative humidity[1], measured with a humidity sensor TSP01 by Thorlabs, Inc. The longer the sample stays in the chamber, the more hydrated it will be.

We stress the fact that it is fundamental to have a sample as thin as possible, to avoid saturation in the OH stretch part of the IR spectrum.

The last type of sample prepared was lysozyme gel. It was prepared placing a $10\,mg/ml$ lysozyme solution droplet on a clean CaF_2 window and let dry at room temperature. After about one hour, the water has evaporated and only a layer of lysozyme gel remained on the window. The sample is ready by placing a second clean window on top.

Table 2.1 summarises all samples measured with IR spectroscopy besides some details about their preparation procedure.

2.1.3 Procedure

The same procedure has been used for all the measurements done with FT-IR, in order to have more reproducible and coherent data. The protocol described below was designed

[1]The relative humidity RH is the index of the amount of water vapor in a gas-vapor mixture. It is defined as the ratio of the partial pressure of the water vapor in the mixture to the equilibrium vapor pressure of water at a given temperature. It is usually expressed as a percentage. 100% relative humidity means that the air is saturated.

Sample	Description
Water	Milli-Q, purified and deionized water.
Lysozyme solution	10 mg/ml: 10 ml of water and 100 mg of lysozyme powder, weighted with a scale.
Gel	10 mg/ml solution droplet on a window and let it dry at room temperature. After about 1 hour it will be dry, ready for measuring it.
Hydrated lysozyme powder	Powder sample exposed to water vapor.

Tabella 2.1: List of the samples measured with infreared spectroscopy.

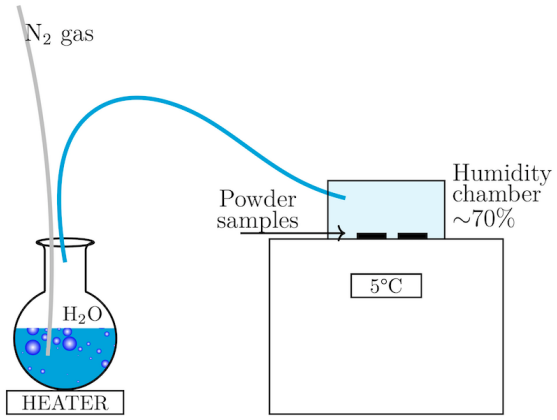

Figura 2.1: Schematic of hydration setup to hydrate protein powder.

to measure each sample at different temperatures, from room temperature to 160 K, and reach thermal equilibrium before measuring and moving to the next temperature.

First of all, we measured the sample at room temperature, T=295 K, and room pressure. Second, we cooled down the sample to T=260 K, below water freezing point, and ran the spectrometer at ambient pressure. After that, we started the vacuum opening a vacuum pump and waited until a pressure of $\sim 5 \cdot 10^{-2}$ mbar was reached. Once a good vacuum was available, we measured the sample at T=260 K. Then, we cooled down the sample to the next temperature, T=250 K, wait five minutes for the thermal equilibrium and scan afterwards. This last step was repeated for all the temperatures until T=160 K. Before each measurement a equilibration time of 5 minutes was utilised based on tests made comparing the temperature measured by two sensors placed in different spots, one the sample mount and one on the sample holder.

Utilizing this procedure, the temperatures at which we measured the samples were between 160 and 260 K with a step of 10 K under vacuum, as well as room temperature at ambient pressure. The ramp rate set in the temperature controller was 5 K/minute. Concerning FT-IR setting, we scanned the frequency interval of $\bar{\nu} = 1200 - 5800\,\mathrm{cm}^{-1}$ for

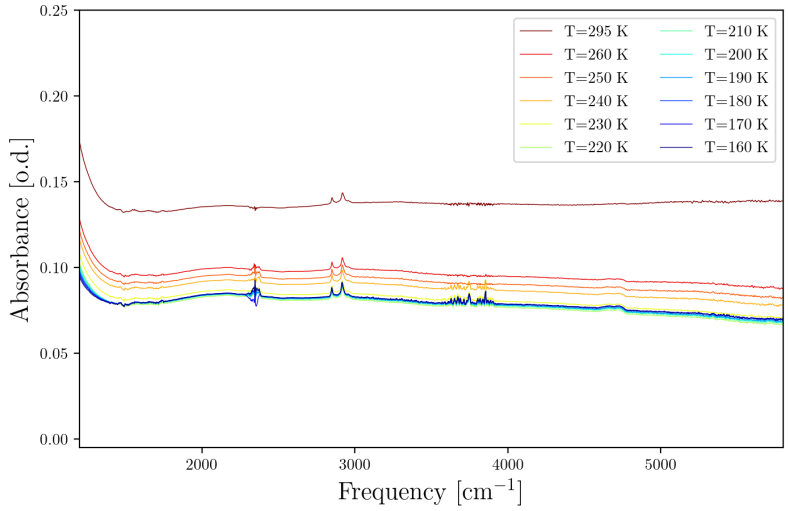

Figura 2.2: Calcium fluoride windows absorbance infrared spectra at different temperatures used as background.

one minute, corresponding to 10 scans, with a resolution of 4 cm^{-1}. In order to acquire the spectra of samples in the liquid phase under vacuum it would have been necessary to seal the windows to prevent loss caused by the vacuum pump. Therefore, it was chosen to take the measurements under vacuum in the solid phase, to avoid this issue. This did not affect the investigation as the protein dynamic transition is expected near 220 K.

The software to control the spectrometer allowed to correct the spectra acquired for the atmospheric suppression, which means that the noise caused by H_2O and CO_2 gas vibrations was automatically corrected. In order to further reduce the noise, nitrogen gas was flowed inside the sample compartment of the spectrometer. However, some noise was still affecting the spectra, as will be highlighted in the results discussion (chapter 3).

Regarding the data analysis, the same background subtraction was made for all datasets. More specifically, the absorbance spectra of two CaF_2 windows over the temperature range T=160-295 K was taken following the procedure described above, as the windows expands varying the temperature and, as a consequence, their absorbance changes. Then, we subtracted the background, i.e. the CaF_2 spectrum, to the sample measurement removing its offset, as the baseline of the spectra depends on the sample thickness. This subtraction was done for all temperatures. The CaF_2 spectra at different temperatures are displayed in figure 2.2.

2.2 X-ray diffraction

X-ray diffraction is a widely used technique for studying the structure of crystalline solids. However, it can also be utilized to investigate amorphous materials, as in the present case.

In X-ray scattering, the incident electromagnetic waves are scattered by the electrons of the probed material, which we refer to as scatterers, and the electromagnetic waves change their direction of propagation. The interaction does not involve energy exchange

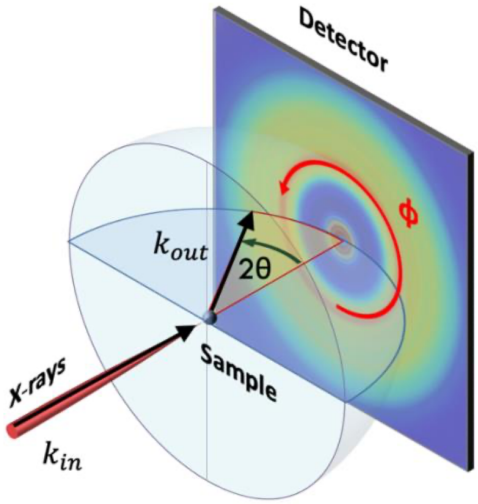

Figura 2.3: Schematic of X-ray diffraction setup showing how the diffraction pattern is obtained [56].

since the photon energy is much smaller than the mass energy of the scatterers, thus the scattering is classified as elastic.

The outgoing electromagnetic waves have different optical paths, as the waves are scattered by different lattice planes of the material, so they interfere with each other forming constructive and deconstructive interference. The brighter spots detected corresponds to the so-called Bragg peaks, described by the Bragg's law

$$n\lambda = 2\,d\,\sin(\theta) \tag{2.5}$$

where λ is the wavelength of the incident beam, d is the distance between the lattice planes of the sample, θ is the scattering angle and n is an integer number. In other words, when the difference of the optical paths given by the lattice planes is an integer multiple of the wavelength there is constructive interference. Then, we define the quantity momentum transfer Q as the difference of the wavevectors between the incident and the outgoing waves

$$Q = |\vec{k}_{out} - \vec{k}_{in}| \tag{2.6}$$

We stress the fact that, as in the inelastic scattering process the energy is conserved, the wavevectors of the incident and outgoing electromagnetic waves are equal in module and only their direction changes.

The measurements done by means of X-ray diffraction provide a two-dimensional diffraction pattern characterized by Bragg peaks in the case of crystalline samples and by diffuse rings in the case of amorphous materials, such as aqueous solutions and hydrated protein powder samples where the constituting molecules have random orientations. The position of the Bragg peaks or the rings reflect the reciprocal space from which one can obtain information about the direct space of the materials, or, in other words, about the structure. A schematic of the X-ray diffraction setup is provided in figure 2.3.

Two-dimensional patterns are usually converted to one-dimensional angular integrated intensities in order to obtain the scattered intensity I as a function of the momentum transfer Q, computed using the equation

$$Q = \frac{4\pi}{\lambda} \sin(\theta). \tag{2.7}$$

This means that higher scattering angles, that is higher Q, in the reciprocal space correspond to smaller structures in the real space, justified by equations 2.5 and 2.7. In summary, the present technique can be utilized for measuring the spacing between planes of atoms and determining the orientation of crystals as well as to study the structure of an unknown materials.

2.2.1 Experimental setup

The X-ray diffractometer used was a Single crystal XRD D8-Venture manufactured by Bruker Corporation. It is simultaneously equipped with two sources of radiation, Molybdenum (Mo) and Copper (Cu). In our particular case, the latter has been used. The beam is directed to the sample placed on a sample holder, and centered by means of a CCD camera for positioning, with the possibility to rotate it thanks to a goniometer. A beam blocker was used to stop the direct beam that might damage the detector. The detector Shutterless PHOTON 100 CMOS was used, with a 1024x1024 pixels of 96 μm edge. The setup was completely controlled by APEX3 software. Moreover, the diffractometer was also equipped with Oxford Cryosystems 700 Series Cryostream Cooler; its nitrogen flow allows to measure at temperatures from 80 to 400 K. As the environment is not under vacuum, a dry airflow prevents ice building around the sample when cool temperatures are set.

The samples are prepared inside thin capillaries made of Kapton®, a polyimide film developed by DuPont and purchased by Goodfellow Cambridge Ltd (product number IM307100/7), with 1.05 mm of external diameter, 1.0 mm of internal diameter and 0.025 mm of wall thickness. In addition, silver behenate has been chosen for the Q-calibration, as its diffraction pattern features several rings, suitable for precise calibration (figure 2.4).

2.2.2 Sample preparation

All the samples were prepared similarly to the case of FT-IR. Afterwards, the capillaries were filled and sealed with epoxy paste. It is worth noting that in the case of liquid samples, both ends must be open, otherwise the liquid could not flow inside because of water capillary action. On the other hand, when dealing with protein powder, one side of the capillary was sealed to prevent loss.

Moreover, hydrated protein powder was prepared in a closed chamber with a high humidity level, as described in 2.1.2, with the only difference that the protein powder was placed on small dishes instead of windows and after hydration the capillary was filled.

Last, the lysozyme gel was prepared pouring a 10 mg/ml lysozyme solution inside a capillary and let dry overnight in the oven at 30° to hasten the process. The procedure was repeated three times in order to obtain a thicker sample.

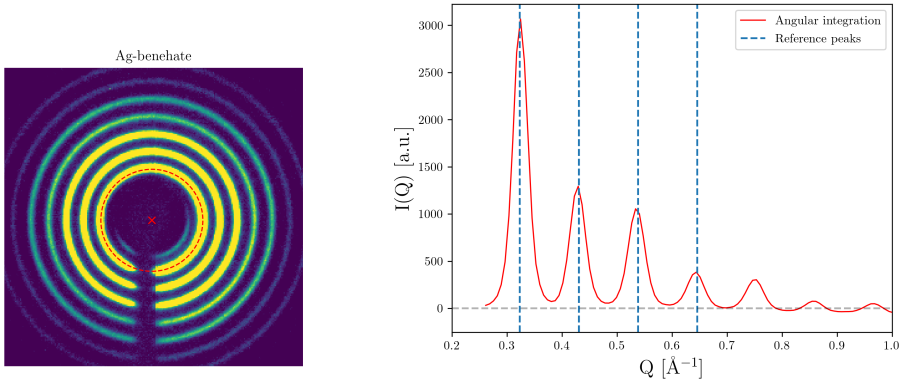

(a) Two-dimentional diffraction pattern showing the center and first ring computed with a Python code.

(b) Angular integrated intensity as a function of the momentum transfer and reference values of Ag-behenate peaks.

Figura 2.4: Q calibration of X-ray diffraction patterns done with silver behenate.

2.2.3 Procedure

For each measurement session, the same settings have been used. In particular, the source used was Copper Kα radiation with a wavelength of λ=1.54 Å and energy E = 8041 eV. The sample-detector distance was set at 50 mm and each measurement was carried out with an exposure time of 100 seconds.

At the beginning of each measurement, silver behenate was first measured as a calibrator, shown in picture 2.4, followed by the background, that is empty Kapton® capillary (figure 2.5). Afterwards, all room temperature measurements were done with the same settings as before. Then, we measured the samples at different temperatures starting from room temperature to low temperatures with steps of 10 K. The ramp rate was set at 360 K/hour and after each temperature was reached we waited five additional minutes for the thermal equilibrium.

In order to estimate the temperature error, some tests based on water melting point were conducted. The temperature error estimated was ±5 K.

Concerning the data analysis, the background was subtracted to all datasets using the same procedure. Specifically, the diffraction pattern of the empty Kapton® capillary was taken and subtracted to all subsequent measurements in a weight manner. The reason why we weighted the subtracted background is because depending on the spot where the sample was hit by the incident beam, the sample thickness might vary as capillaries have circular section. Thus, the background is slightly different for each sample measured. Furthermore, to calculate the angular integration of the scattering pattern, a mask was used to cover the beam blocker and to avoid the non uniform intensity at high Q due to the detector edges. Figure 2.5 shows the angular integrated intensity of the background (Kapton®) as a function of the momentum transfer with two peaks at Q=0.41 Å^{-1} and Q=1.34 Å^{-1}.

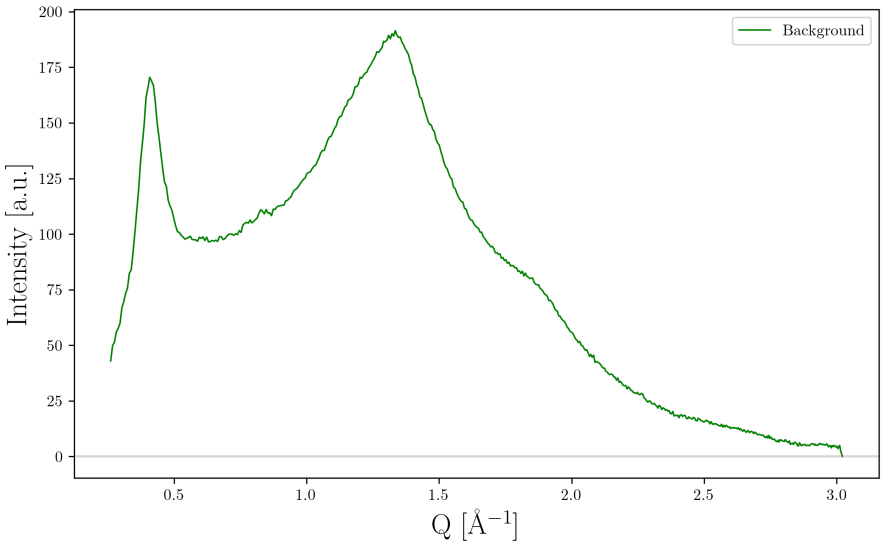

Figura 2.5: Angularly integrated intensity of the Kapton® capillary used as background in XRD measurements. One peak is at $Q \sim 0.41\,Å^{-1}$ and the second peak at $Q \sim 1.34\,Å^{-1}$.

Capitolo 3

Results and discussion

In this chapter the experimental results of the investigation on the lysozyme dynamic transition are presented. The first section reports the results obtained by means of infrared spectroscopy, whereas the second section focuses on X-ray diffraction measurements and results.

3.1 Fourier transform infrared spectroscopy

3.1.1 Pure water

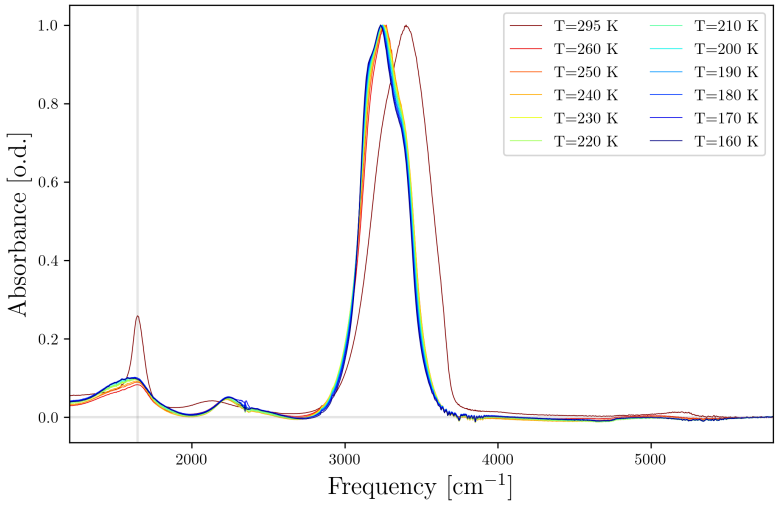

Figura 3.1: Pure water absorbance spectra at T=160-295 K normalized to the highest peak corresponding to OH-stretching modes.

Figure 3.1 represents the infrared absorbance spectrum of pure water as a function of frequency and how it changes as the temperature is decreases from 295 K to 160 K. The two main regions of interest are found within the frequency interval 2800-3800 cm^{-1}, related to OH-stretching modes, and 1400-1800 cm^{-1}, related to OH-bending mode. In the following, we compare these two intervals for water and lysozyme solution (10 mg/ml

of concentration) absorbance spectra as well as hydrated lysozyme powder. All presented spectra are normalized with respect to the highest peak of OH-stretching modes. The water vibrational frequencies of the water molecule in the liquid phase are reported in table A.1 of appendix A.

Starting with the OH-stretch, figure 3.1 shows the phase transition from liquid (dark red line) to solid state, where the the peak redshifts by $\sim 150\,\mathrm{cm}^{-1}$ upon freezing the sample from a temperature of 295 K to 260 K. It redshifts further upon decreasing the temperature to 160 K, although relatively less. By decreasing the temperature the hydrogen bond strengths become higher, lowering the OH-stretch frequencies. Further, the line shape of the OH-stretching mode exhibits three contributions observed as shoulders in the spectrum, better resolved in the solid phase, caused by the intramolecular and intermolecular coupling. Two shoulders at $3277\,\mathrm{cm}^{-1}$ and $3490\,\mathrm{cm}^{-1}$ are associated to the symmetric and antisymmetric vibrational modes of the water molecule (ν_1 and ν_2), while the third shoulder is related to the HOH bending overtone mode [22]. Recent studies attribute the line shape at lower frequencies to the low-density liquid, whereas the line shape at higher frequencies is associated with the high-density liquid water [38] [33].

The OH-bend region (1400-1800 cm^{-1}) is broadened by freezing, since the water molecules are constrained in the crystalline configuration of crystalline ice with reduced bending amplitude because of hydrogen bonds [45] [36].

Moreover, the interval 1800-2800 cm^{-1} is called 'combination band' arising due to the superposition of librations and OH-bending modes. The fluctuations near 2300 and $3700\,\mathrm{cm}^{-1}$ are caused due to the absorption of carbon dioxide and water molecules in the air [56].

3.1.2 Hydrated lysozyme powder

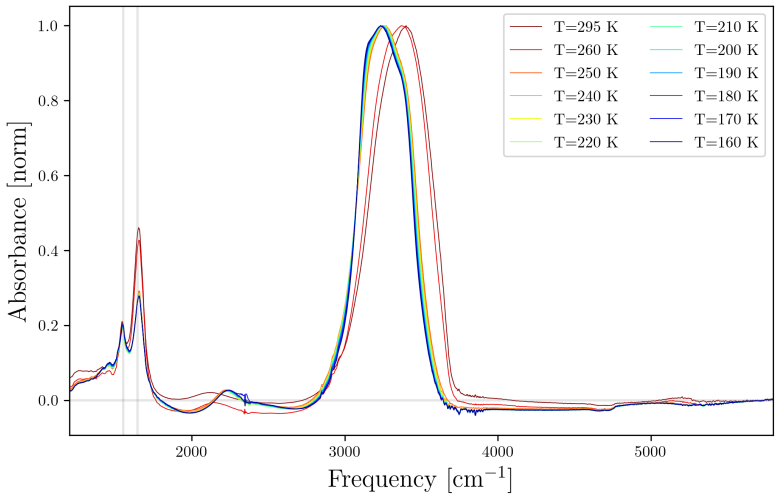

Figura 3.2: Hydrated lysozyme powder absorbance spectra at T=160-295 K normalized to the highest peak corresponding to OH-stretching modes.

The results of hydrated lysozyme powder probed with infrared spectroscopy are shown in figure 3.2. The main difference with respect to water regards the OH-bend region. Indeed, hydrated lysozyme powder presents additional peaks associated to vibrational modes of the secondary structure of the protein, called Amide [41]. Amide modes are often divided into three contributions, Amide I, II and III, each of them caused by a superposition of different modes described in table A.2 in appendix A [34]. Confined and hydration water are in general more likely to be supercooled than bulk water [16], however here the liquid-solid transition clearly happens between 260 and 250 K. This means that the hydration water cannot be supercooled due to its too large amount.

OH-stretch and OH-bend regions are shown in figure 3.3b and 3.3a respectively, comparing pure water (dashed lines) and hydrated lysozyme powder (solid lines) at room temperature (red curves) and 250 K (blue curves). As well as the occurring liquid-solid phase transition and the presence of Amide I and II peaks, in figure 3.3b we observe a difference in the line shapes [38] [33]. Considering the recent interpretation of the line shapes, at room temperature the hydrated lysozyme powder shows a more prominent contribution of the low-density phase.

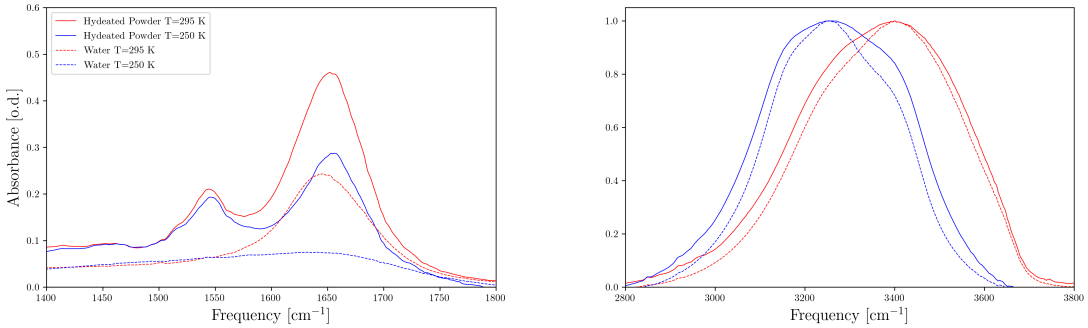

(a) OH-bending region *(b) OH-stretching region*

Figura 3.3: Hydrated lysozyme powder (solid lined) and pure water (dashed lines) absorbance spectra at T=250 K (blue curves) and T=295 K (red curves).

Figure 3.3a displays the OH-bend and Amide region of the absorbance spectra. As already mentioned for figure 3.1, water shows a broadening in OH-bending mode by freezing. Lysozyme, on the other hand, presents the additional Amides. Note that the main peak of lysozyme in this spectral region is a superposition of OH-bend and C=O stretching mode of its secondary structure; this explains the reason for the apparent blueshift of the main peak and its reduced intensity in the solid phase.

3.1.3 Dry lysozyme powder and lysozyme gel

We then measured dry lysozyme powder and lysozyme gel, whose preparation procedure is described in section 2.1.2, and the infrared absorbance spectra at room temperature are shown in figure 3.4, normalized with respect the Amide I peak. The gel exhibits a triangular shaped peak at the OH-stretching frequency mode as well as two sharp peaks at amide frequencies in agreement with hydrated lysozyme powder.

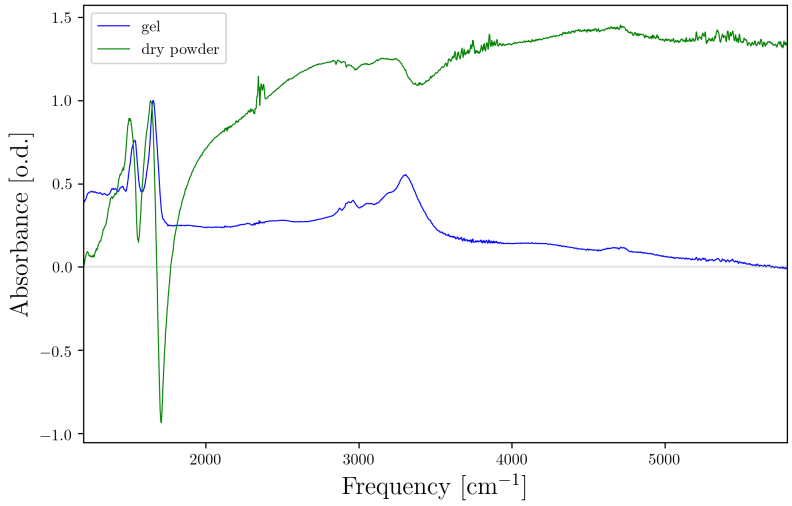

Figura 3.4: Lysozyme gel (blue) and dry lysozyme powder (green) at T=295 K.

Dry lysozyme powder is characterized by a high baseline, caused by the sample thickness. Indeed, the solid sample made of protein powder was grinded to reduce the particles size, however, the grains were still large. Despite this, it is possible to obtain some valid information from the spectrum. Dry lysozyme powder spectrum features the two amide peaks, which are redshifted by $\sim 20\,\mathrm{cm}^{-1}$ with respect to what expected. Hence, Amide I and Amide II are slowed down when dehydrated. Then, at the OH-stretch mode frequency, dry powder exhibits a dip. Moreover, at $1700\,\mathrm{cm}^{-1}$, dry powder manifests a negative dip which could be caused by the constructive interference, giving a higher total output intensity. The beam with a wavelength of $5.8\,\mu$m might scatter within the sample, specifically within the gaps between the lysozyme grains with the same length scale as the wavelength, resulting in an interference.

Dry lysozyme powder and lysozyme gel infrared spectra taken over a temperature range 160-295 K are reported in appendix C and it is possible to note that the spectra do not change as the temperature varies. Thus, lysozyme dynamics do not exhibit any change in dry environments.

3.1.4 Hydrations estimations

The next section of the analysis was concerned with the ratio of OH-stretch to Amide I and the ratio of OH-stretch to Amide II for two hydrated lysozyme powder samples with different hydrations and lysozyme solution with 10 mg/ml of concentration. The aim was to estimate the h value of hydrated lysozyme powder. In figure 3.5 we report the values obtained (dots) together with the known theoretical value for 10 mg/ml solution (cross).

In the case of lysozyme solution, the amount of hydration is known and can be obtained by the concentration 10 mg/ml. Hence, $h = 100$. By computing the ratio of OH-stretching and Amide II absorbance, we get $h \approx 86$, with 16% of discrepancy. Whereas, by computing the ratio of OH-stretching and Amide I absorbance, the result is $h \approx 38$, which is far from

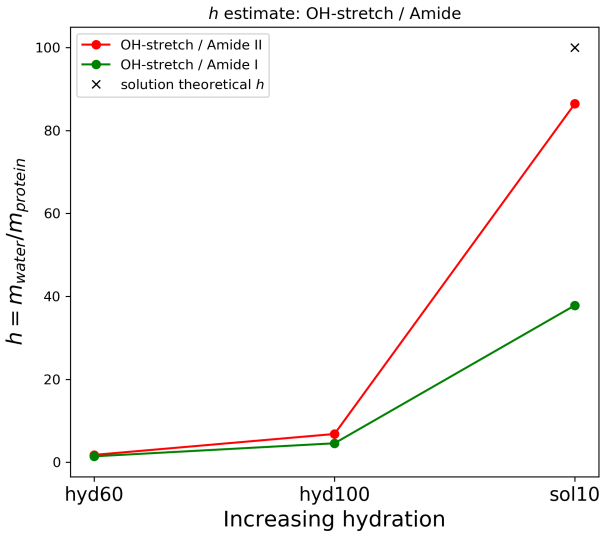

Figura 3.5: Estimations of hydration value h, defined in eq. 1.1, for lysozyme solution 10 mg/ml (sol10 in the horizontal axis) and hydrated powder samples, exposed to water vapor for 60 (hyd60 in the horizontal axis) and 100 minutes (hyd100 in the horizontal axis). The level of hydration is estimated by computing the ratio of OH-stretching mode to Amide I or II absorbance values.

the theoretical value. Hence, we can conclude that the ratio of OH-stretching to Amide II absorbance values is more consistent with the theoretical value of 10 mg/ml lysozyme solution. It may be due to the fact that the Amide I and OH-bend mode are difficult to separate, while Amide II peak is not as affected by water as Amide II, therefore it gives a better estimation of the hydration value.

With this reasoning we estimate the hydration for the hydrated lysozyme powder samples we measured. As depicted in figure 3.5, for the sample exposed to water vapor for 60 minutes has $h_{60\,min} = 1.8$, while the hydration level of the sample exposed for 100 minutes to water vapor has $h_{100\,min} = 6.8$. Based on the comparison of the theoretical and experimental hydration h for lysozyme solution, we found that the discrepancy is $\sim$ 16%. Therefore, this method provide a rough estimation of the amount of hydration of the samples measured, however improvements on the data analysis will help to obtain better estimates.

3.2 X-ray diffraction

3.2.1 Lysozyme solutions

The two-dimensional diffraction patterns produced by means of X-ray diffraction of the measured samples, presented in figure 3.6, are characterized by diffuse rings of scattered intensity. More specifically, we show the patterns of pure water, lysozyme solution with a concentration of 300 mg/ml on the left column and dry and hydrated lysozyme powder on the right column. The direct beam is stopped by a beam blocker masked in the

data analysis. The rings result from the random orientation of molecules and amorphous structure, as already described in section 2.2.

Water shows a single diffraction ring in the available Q range, precisely at Q=2 $Å^{-1}$. It is caused due to the scattering by the oxygen atoms. In the case of lysozyme solution, although the diffraction pattern is dominated by the same diffraction ring at 2 $Å^{-1}$ as in the case of pure water, an additional weaker is also noticeable at low momentum transfer. The same ring at smaller momentum transfer is present and prominent in the case of both dry and hydrated lysozyme powder. Therefore, the additional peak must be related to the protein structure.

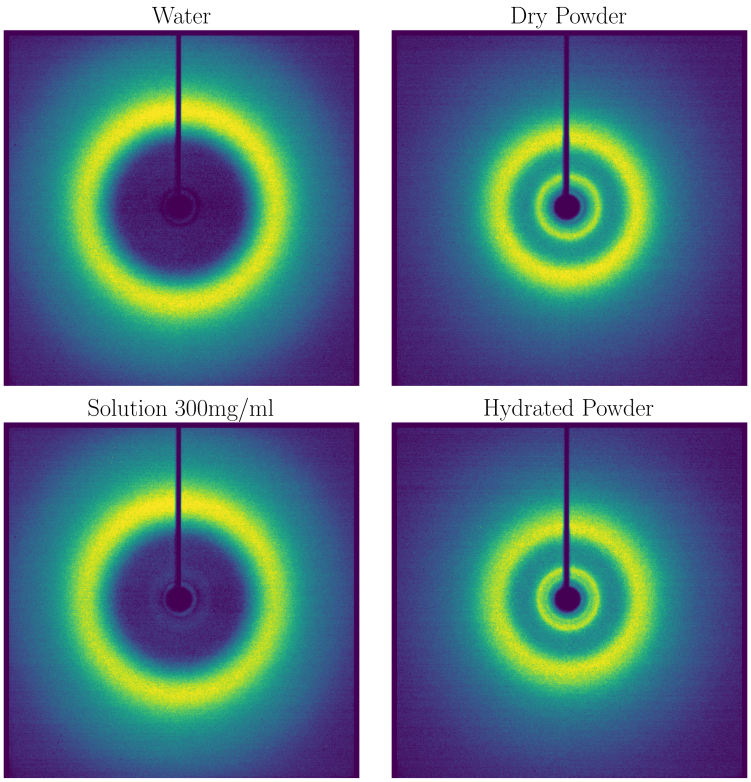

Figura 3.6: Two-dimensional diffraction pattern of water (top left), dry lysozyme powder (top right), lysozyme solution of 300 mg/ml concentration (bottom left) and hydrated lysozyme powder (bottom right).

Lysozyme solutions with different concentrations (100, 200, 300 mg/ml) were measured and the angular integrated intensities vs momentum transfer are displayed in figure 3.7 compared to water and dry lysozyme powder (dashed curves). Here, the low-Q peak at ∼0.62 $Å^{-1}$ mentioned is clearer: the more the solution is concentrated, the more the intensity grows. Note that all the curves are normalized with respect to the high-Q peak. The low-Q peak becomes prominent for dry lysozyme powder, visible both in the diffraction pattern (figure 3.6c) and in the angular integration (figure 3.7 black dashed line). This bolsters the hypothesis that it is a diffraction caused by the protein. Furthermore, the intensity of the dry powder has a peak at ∼1.41 $Å^{-1}$ with an amplitude comparable to the amplitude of the low-Q peak. According to simulations made by Svergun et al. [51],

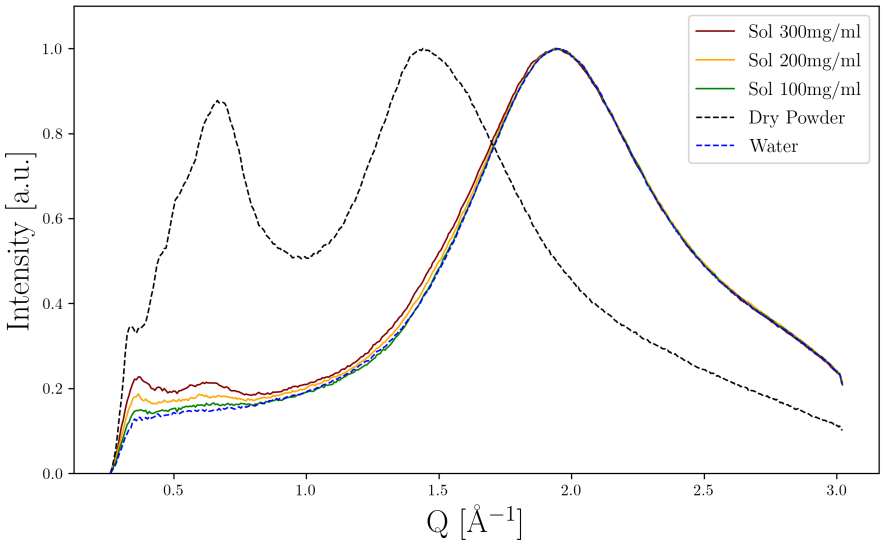

Figura 3.7: Angularly integrated intensity of water (blue dashed curve), lysozyme solutions with different concentrations (100, 200, 300 mg/ml solid lines) compared to dry lysozyme powder (black dashed curve). All the curves are normalized to their highest peak.

the peak is connected to the characteristic interatomic distances in α helices of the protein secondary structure. The same contribution might cause the enhancement in the water peak rising part of the solutions with respect to pure water.

3.2.2 Dry and hydrated lysozyme powder at different temperatures

In order to investigate a potential variation of the protein structure with temperature, we measured the samples from T=295 to T=180 K with the procedure described in section 2.2.3. Dry lysozyme powder angular integration as a function of the momentum transfer at temperatures from 180 to 295 K is displayed in figure 3.8. All the curves are normalized with respect to the highest peak, in figure 3.8 and all the following figures displaying angular integrated intensities (figures 3.11-3.12). We recognize that the shoulder in the falling part of the high-Q peak grows as the temperature decreases. The opposite behavior is observed for the peak at Q$\sim$0.62 Å^{-1}: the amplitude decreases as the temperature is cooled down. In appendix C.2 the dry lysozyme powder integrated intensities are shown with a normalization done with respect to the low-Q peak.

The same temperature variation was carried out for hydrated lysozyme powder, which is presented in figure 3.9 and compared with dry powder (dashed line). There is a striking difference in the high-Q peak: the protein powder shifts by $\sim$0.06 Å^{-1} towards higher momentum transfer when hydrated. In addition, the shoulder at $\sim$2 Å^{-1} is more pronounced with respect to the dry powder. We relate it as the contribution of the liquid water present in hydrated powder but absent is the dry powder. Concerning the peak at $\sim$0.62 Å^{-1}, we note that for hydrated powder its amplitude sinks more as the temperature decreases than the dry powder. In appendix C.2 the hydrated lysozyme powder integrated intensities are shown with a normalization done with respect to the low-Q peak.

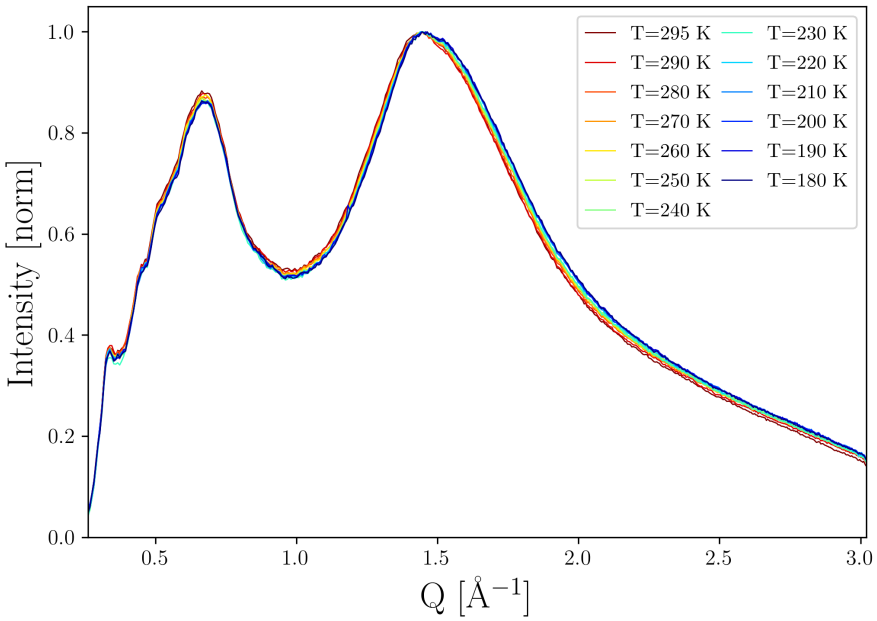

Figura 3.8: Angularly integrated intensity of dry lysozyme powder at temperatures from 180 to 295 K normalized to the highest peak.

Our goal was to observe the behavior of hydrated lysozyme powder with different hydration levels over temperature. A second sample of hydrated powder was measured with a higher hydration level (figure 3.10). What differentiate the hydrated lysozyme powder of figure 3.10 from the sample shown in figure 3.9 is mainly in the conditions under which the protein powder was hydrated. More specifically, in the case of figure 3.10, the average relative hydration inside the humidity chamber was ∼80%, while in the case of figure 3.9 it was ∼70%. The shoulder at ∼2 Å^{-1} due to water molecules is much more evident than in figure 3.9. However, cooling between 260 K and 250 K, the hydration water freezes showing the characteristic sharp peaks of crystalline ice (Ih). Because of freezing, it is not possible to compare the hydrated protein structure down to 180 K, nowever the same behavior of the high-Q peak is noticeable before the hydration water freezes: both the shift of ∼ 1.5 Å^{-1} towards higher momentum transfer and its rising shoulder near 2 Å^{-1}.

In order to better compare the effect of hydration to protein powder, we present in figure 3.11 the angular integrated intensities of hydrated lysozyme powder samples with different hydration levels reached by exposing the dry powder to water vapor for different amount of time, 30 minutes (red curve) and 1 hour (blue curve) with 70% of relative humidity, and 1 hour (green curve) with 80% of relative humidity. The hydrated powders are compared to dry powder (dashed curve); all the measurements were taken at room temperature. In accordance with figure 3.9 and 3.10, the high-Q peak shift is reproduced for all hydrated powders depicted in figure 3.11 as well as the enhanced shoulder originated by water molecules present in the samples. Further, the low-Q peak shows a higher amplitude in the case of hydrated powder with respect to dry powder as already observed in figure 3.9 and 3.10.

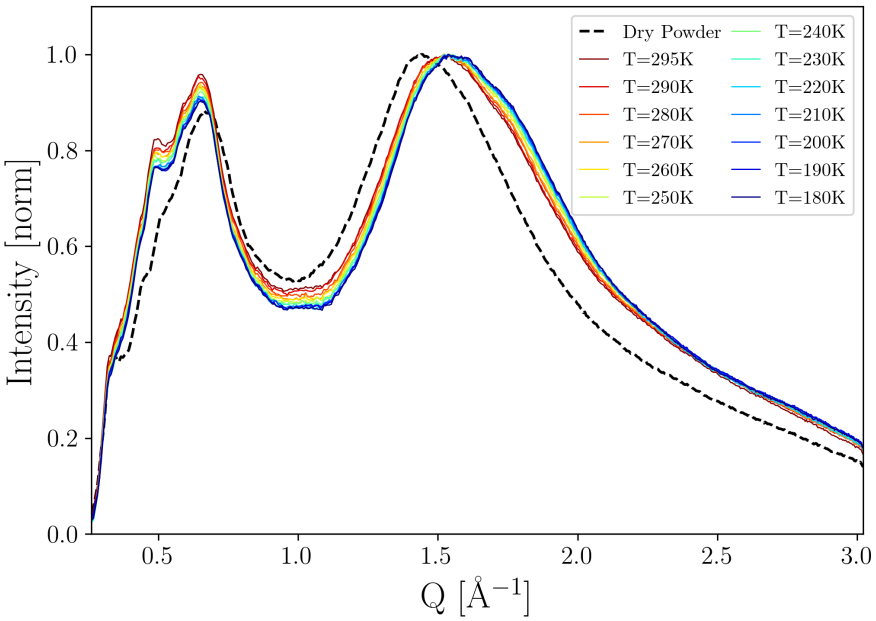

Figura 3.9: Angularly integrated intensity of hydrated lysozyme powder at temperatures from 180 to 295 K compared to dry lysozyme powder at T=295 K (black dashed line). All the curves are normalized to their highest peak. The hydrated lysozyme powder sample was prepared by hydrating the dry lysozyme powder for one hour with ∼ 70% of relative humidity.

A comparison of figures 3.8-3.10 reveals also that an additional peak at ∼0.44 Å^{-1} appear more prominent for higher hydrations. However, a careful analysis must be done concerning the background subtraction as the peak caused by the capillary material is at Q=0.41 Å^{-1}, which might affect the low-Q region.

As can be seen from figure 3.12, the lysozyme gel integrated intensity as function of the momentum transfer has a similar shape as dry lysozyme powder, meaning that, from a structural point of view, dry lysozyme and gel are equal, maintaining their secondary structures probed by means of X-ray diffraction.

3.2.3 Hydration water

From figures 3.9-3.11, we observed that the shoulder of the peak at higher momentum transfer seems to be related to the water present in the sample, that is hydration water. Being confined, hydration water is believed to behave differently to bulk water. So, it is interesting to compare hydration and bulk water, as shown in figure 3.13, where the scattering intensity as a function of the momentum transfer of hydration water is plotted at variable temperatures, from 180 to 295 K (colored lines), and compared to bulk water at 295 K (black line). Hydration water is obtained by subtracting dry lysozyme powder scattering intensity from the hydrated lysozyme powder one for each temperature. We observe that hydration water is shifted towards lower momentum transfer by $\Delta Q = 0.14$ Å^{-1} with respect to bulk water.

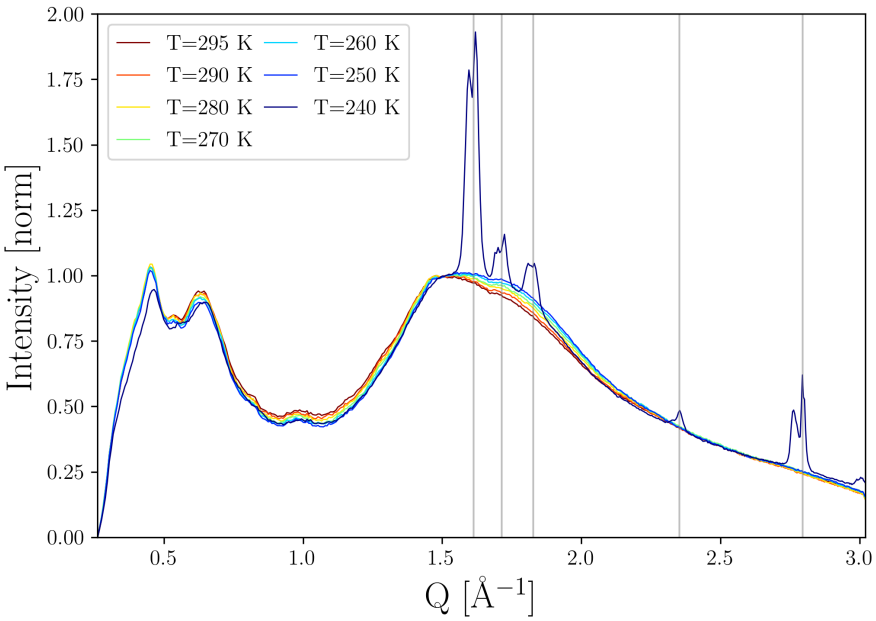

Figura 3.10: Angularly integrated intensity of hydrated lysozyme powder at temperature from 250 to 295 K showing frozen hydration water at 250 K. All the curves are normalized to their highest peak. The hydrated lysozyme powder sample was prepared by hydrating the dry lysozyme powder for one hour with ∼ 80% of relative humidity.

Sellberg et al. [49] measured pure water droplets at different temperatures with X-ray scattering and observed that the intensity peak centered near ∼2 Å^{-1} is shifted towards lower momentum transfer as the temperatures decreases. According to the two phases of liquid water hypothesis, water goes from high-density to the low-density liquid phase from room temperature towards cooler temperatures. Thus, they interpret the peak located at lower Q as the signature of low-density liquid water. In this scenario, hydration water of hydrated lysozyme powder samples seems to be more LDL-like, in agreement with FT-IR measurements previously shown in section 3.1.2. In contrast to Sellberg et al. results, hydration water does not significantly shift upon changing the temperature. This may be explained by the fact that hydration water is confined water, and shows different thermodynamic properties to that of bulk water [35] because water molecules are arranged around the protein surface and act as a bridge between proteins, forming different hydrogen bond network.

The shoulder of hydration water at ∼1.5 Å^{-1} is sensitive to the subtraction, because dry and hydrated lysozyme are slightly different from a structural point of view, as already underlined in the previous sections. It would be interesting to compare the scattering intensity obtained experimentally (figure 3.13) to that obtained from molecular dynamics simulations and which can provide a further insight in to the hydrogen bond properties of hydration water.

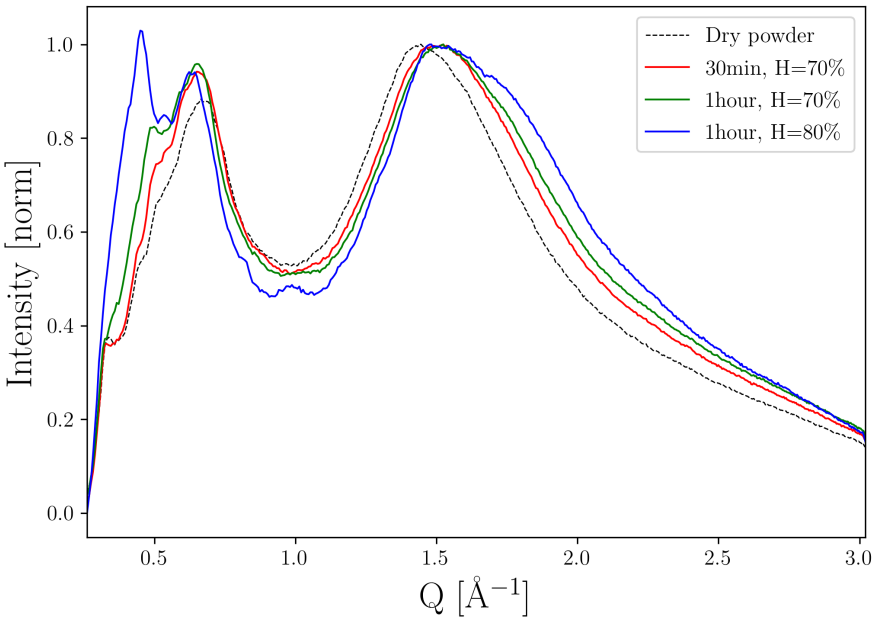

Figura 3.11: Angularly integrated intensity of hydrated lysozyme powder samples with different hydration levels at room temperature (solid lines) compared to dry lysozyme powder (black dashed curve). All the curves are normalized to their highest peak. The hydrated lysozyme powder sample represented by the red curve was exposed to water vapor for 30 minutes with a relative humidity of ∼ 70 %. The hydrated lysozyme powder sample represented by the green curve was exposed to water vapor for one hour with a relative humidity of ∼ 70 %. The hydrated lysozyme powder sample represented by the blue curve was exposed to water vapor for one hour with a relative humidity of ∼ 80 %.

3.2.4 Protein crossover

Figure 3.14 shows the ratio of the low-Q and high-Q peak amplitudes as a function of temperature for all datasets. The errors are calculated based on the Q resolution. What stands out in figure 3.14 is the abrupt slope change near T∼230-240 K, both for dry and hydrated powder. It is worth mentioning that the error of the temperature was estimated to be ±5 K with previous tests based on water melting point (section 2.2.3). The crossover could be attributed to the protein structure since it is clear also for dry protein powder. However, the hydrated protein shows an enhanced change, thus indicating hydration water plays a role in the behavior described by figure 3.14. The hydrated protein powders in figure 3.14 correspond to two samples prepared and measured in two different days with the same exposure time, i.e. one hour, under the same experimental conditions, which was done to test reproducibility. In addition, the same behavior was observed for measurements carried out from cool to warm temperatures (shown in appendix C.2). Further, computing the ratio discards any normalization issues. The raw data are reported in table D.1 of appendix D.

Figure 3.15 shows the centers of the high-Q peak of dry and hydrated powder and reported with the temperature dependence. The centers and their uncertainties are obtai-

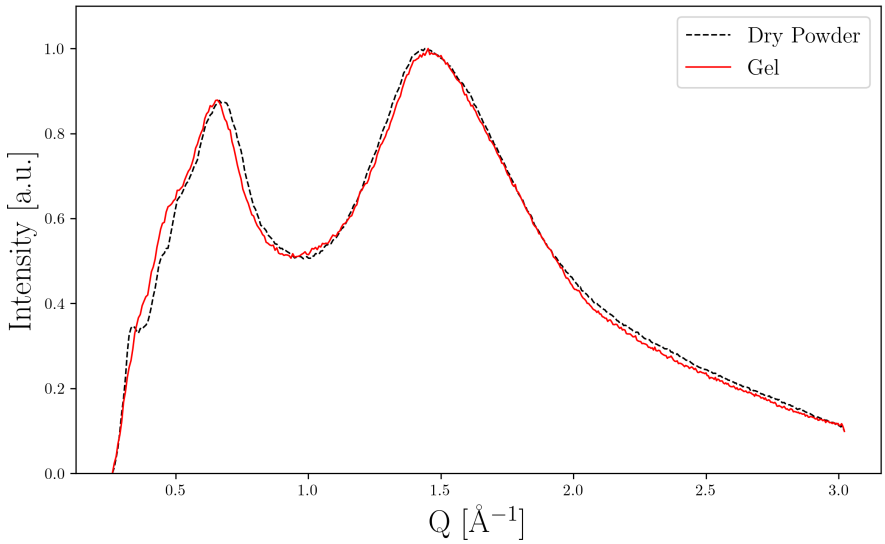

Figura 3.12: Angularly integrated intensity of lysozyme gel (red solid line) and dry powder (black dashed line) at room temperature. Both curves are normalized to the highest peak.

ned by fitting the peak with a Voigt distribution. The measurements were taken during the same day using the same procedure, as explained in section 2.2.3. Both samples measured show a comparable trend: upon decreasing the temperature the peak shifts towards higher momentum transfer, before reaching a plateau at and below 240 K. Nevertheless, as already observed in figure 3.9-3.11, the shift of hydrated lysozyme powder with respect to dry powder is clear and it is estimated to be $\sim$0.06 Å^{-1}.

Note that, it might be possible that some residual hydration is present in the dry lysozyme powder due to the air exposure during the sample preparation, since the sample was prepared without any further drying process.

The raw data are reported in table D.2 of appendix D. An attempt of hydration estimate was done by weighting the lysozyme powder before and after the hydration process. However, the amount of hydration water was too little to weigh with a scale, making direct estimation of hydration level difficult.

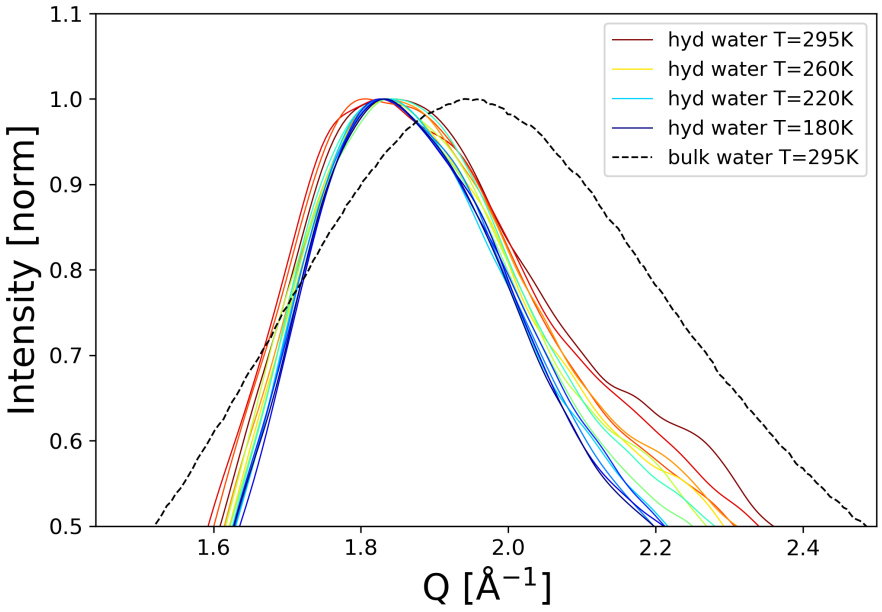

Figura 3.13: Angularly integrated scattering intensity of hydration water at different temperatures, from 180 to 295 K (colored lines), compared with bulk water at 295 K. All the curves are normalized to their highest peak.

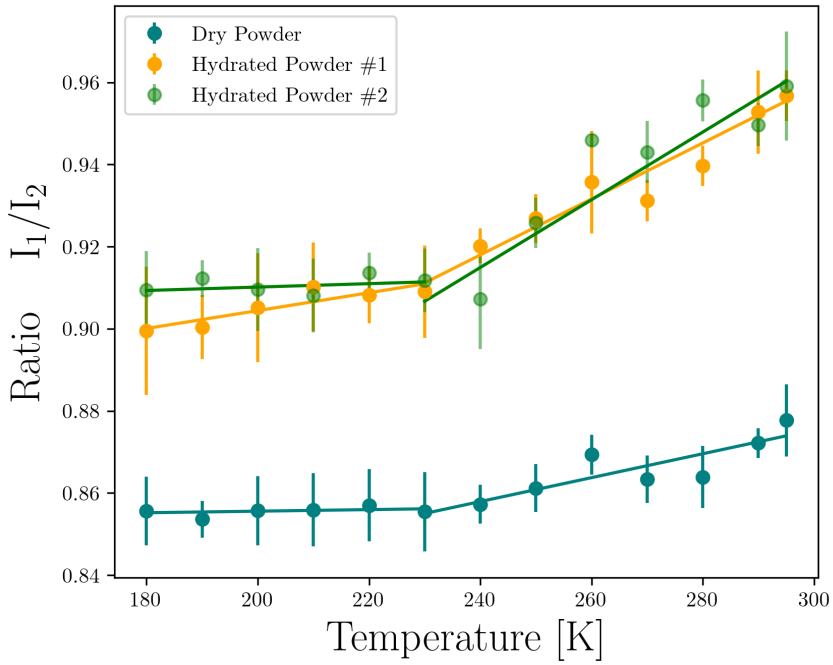

Figura 3.14: Ratio of the maxima of $Q \sim 0.62\,\AA^{-1}$ and $Q \sim 1.41\,\AA^{-1}$ peaks as a function of temperature, for dry (blue dots) and hydrated (two samples, green and orange dots) lysozyme powder. Both hydrated lysozyme powder samples were prepared under identical conditions, namely exposed to water vapor for one hour with $\sim 70\%$ of relative humidity.

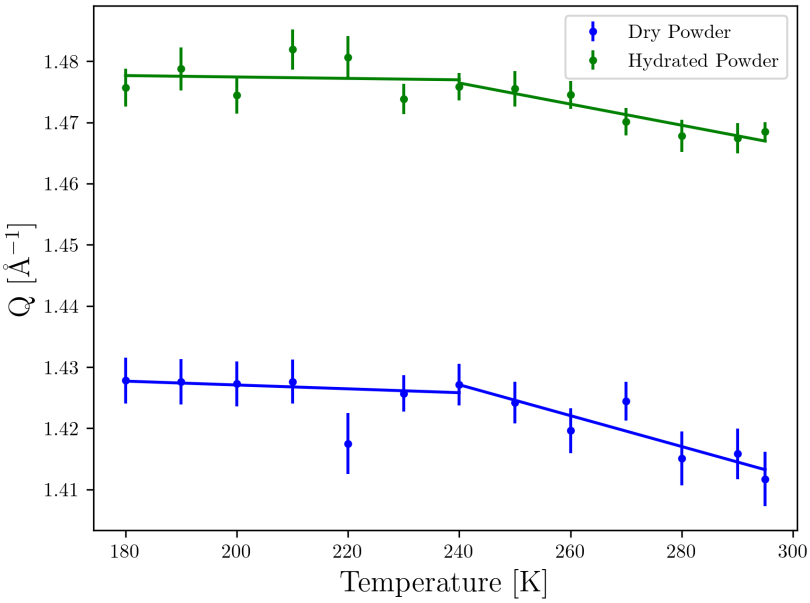

Figura 3.15: Centers of high-Q peak as a function of temperature for dry (blue) and hydrated (green) lysozyme powder. The values with their uncertainty are obtained by fitting the peak with a Voigt distribution.

Capitolo 4

Conclusions and outlook

The aim of this work was to investigate the protein dynamic transition of lysozyme by means of infrared spectroscopy and X-ray diffraction.

We implemented the experimental setup for hydrating protein powder in a controlled manner, which allowed to prepare the samples of hydrated lysozyme powder, and we compared their measurements to the dry lysozyme powder as well as solutions of different concentrations and pure water.

The FT-IR measurements allowed to measure hydrated lysozyme powder comparing its absorbance spectrum to pure water as well as lysozyme solution. We clearly observed the liquid-solid transition for all the samples by the OH-stretching mode redshift, noting that hydration water freezes at lower temperatures than pure water, between 260 and 250 K, with repeated measurements. This demonstrates that hydration water is more likely to be supercooled than bulk water. Furthermore, we observed that the hydrated lysozyme powder line shape in the OH-stretch region shows a more prominent contribution of low-density liquid, i.e. the lowest frequency shoulder of OH-stretching mode, according to one recent interpretation of water OH-stretching modes [38] [33]. Moreover, the measurements carried out for dry lysozyme powder and lysozyme gel show that their absorbance spectra do not change with temperature alteration. This means that in dry environment lysozyme does not exhibit changes in its dynamic. Finally, the amount of hydration quantified by h was estimated by computing the ratio of the OH-stretching mode to Amide II absorbance values, which provides the order of magnitude of the amount of hydration and more precise data analysis might help to obtain better estimates. Future plan will include improvement on the sample preparation, specifically seal the samples in order to measure them from room to cool temperatures under vacuum as well as measure hydrated lysozyme powder with $h \approx 0.3$.

The XRD measurements gave encouraging results. First, we clearly observed the dry lysozyme powder structure characterized by two peaks at $\mathrm{Q} \sim 0.62\,\text{Å}^{-1}$ and $\mathrm{Q} \sim 1.41\,\text{Å}^{-1}$. The former shows a decreased intensity upon decreasing the temperature, enhanced in the case of hydrated lysozyme powder. The rising of this peak was also noted in lysozyme solutions, gradually more evident as the concentration increases. The latter peak shifts by $0.06\,\text{Å}^{-1}$ towards higher momentum transfer when the protein powder is hydrated and its shoulder at $\sim 2\,\text{Å}^{-1}$ becomes more prominent when the temperature decreases. Moreover, the hydration water is shifted towards lower momentum transfer with respect to bulk water. According to the hypothesis of the two phases of liquid water, hydration water

seems to be more low-density liquid-like, in agreement with infrared spectroscopy results. Additionally, the hydration water around lysozyme powder samples freezes if the h value exceeds a certain threshold and reaches bulk-like water, while it remains in the liquid phase for lower h values when it corresponds to a thin layer surrounding the proteins. Further, at room temperature lysozyme gel shows the same structure as dry lysozyme powder, which was also investigated down to 180 K.

The ratio of the two peak intensities plotted as a function of temperatures shows a crossover at 230 K, both for dry and hydrated lysozyme powder. However, hydration water enhanced the slope change, demonstrating that water plays a role in the protein structure. Last, the temperature dependence of the center of the peak at $Q \sim 1.41\,\text{Å}^{-1}$ for dry powder and at $Q \sim 1.47\,\text{Å}^{-1}$ for hydrated protein powder displays a slope change near 230 K both for hydrated and dry lysozyme powder and it underlines the shift of $Q \sim 0.06\,\text{Å}^{-1}$ occurring when the protein is hydrated. The amount of hydration contained in the samples was estimated by weighing the powder before and after the hydration process, nevertheless the scale utilized was not as sensitive as necessary. Future work will include a direct estimate of the hydration h by weighing utilizing a more sensitive scale or, alternatively, utilizing a different instruments such as thermogravimetric analysis (TGA).

We recall that the hypotheses, presented in section 1.3.1, suggest that the protein dynamic transition is either due to the protein free energy landscape (first hypothesis) or to the hydration water. More precisely, the origin of the protein dynamic crossover reflects the water fragile-to-strong dynamic crossover (second hypothesis) or the low-density and high-density liquid phases of water (third hypothesis). Our results show a crossover in the lysozyme structure that occurs at the expected temperature, near 230 K, enhanced by the presence of hydration water. This is an indication that water influences the protein and therefore we can address our future investigation in order to distinguish the mechanism whereby water gives rise to the protein dynamic transition. Moreover, the different line shapes of OH-stretching modes of hydrated lysozyme powder and pure water at T=295 K (figure 3.3b) indicates that the structure of hydration water is different to bulk water. In other words, the hydrogen bond network of hydration water is different to bulk water. The differences might arise from the two liquid phases of water, namely low-density and high-density, as suggested by Mallamace et al. [34], which is in agreement with the third hypothesis.

However, the second and the third hypotheses are not mutually exclusive, since the former is related to the free energy landscape of water, whereas the latter is associated with the structure of water. A simulation study conducted by Tanaka and coworkers connects the fragile and strong behavior with the two low-density and high-density liquid phases of water [50]. On one hand, they propose that at high temperatures water exists in the high-density phase exhibiting an Arrhenius behavior, typical of strong glass formers, meaning that its free energy landscape is characterized by a single minimum. On the other hand, at low temperatures, water exists in the low-density phase exhibiting a strong behavior but with a different minimum in the free energy landscape with respect to the high-density phase. When crossing over the Widom line, liquid water is hypothesized to be a mixture of the two phases showing, in this case, a fragile behavior with multiple minima in the free energy landscape. According to this view, the low-density and high-density liquids underlie the fragile-to-strong dynamic crossover.

In order to distinguish between the second and the third hypothesis, we need to inve-

stigate hydration water with a technique which provides information both on translational dynamics and structure over temperature. Some techniques which might be utilized in the future work include dynamic light scattering (DLS), to analyze the protein dynamics in dilute solutions, and X-ray photon correlation spectroscopy (XPCS) at synchrotron and free-electron laser facilities (XFELs), to investigate the dynamics at a molecular scale with a time resolution of picoseconds and femtoseconds respectively [12] [39]. Moreover, the structure of the hydrated protein can be investigated with small-angle X-ray scattering (SAXS) technique over a large temperature range at lower momentum transfer values. This would give information on protein shape and radius of gyration. Additionally, in order to improve the sample preparation procedure, thermogravimetric analysis might be utilized for a precise estimation of the protein hydration level. Furthermore, molecular dynamics simulations will be helpful to interpret the results obtained with X-ray diffraction and understand the origin of the two characteristic peaks observed in the protein powder. Finally, it is worth investigating different proteins and examining whether the current observations extend to other hydrated biomolecules.

Appendice A

Infrared vibrational modes

Water		
Frequency (cm^{-1})	**Conformation**	**Mode**
1645	ν_2	OH-bending
2150	$\nu_2 + L_2$	combination band
3277	ν_1	symmetric OH-stretching
3490	ν_3	antisymmetric OH-stretching
5260	$a \cdot \nu_1 + \nu_2 + b \cdot \nu_3$, $a + b = 1$	combination band

Tabella A.1: Liquid water vibrational modes [31].

Protein secondary structure		
Frequency (cm^{-1})	**Conformation**	**Mode**
	Amide I	
1680-1696	Antiparallel β-sheets	C=O stretching
1655-1875	Random coil	C=O stretching
1650-1657	α-helix	C=O stretching
1612-1630	Antiparallel β-sheets	C=O stretching
	Amide II	
≈1540	Peptide backbone	N-H bending
≈1520	Peptide backbone	C-N bending
	Amide III	
1220-1400	Superposition of different bands	N-H bend + C-N stretch, C-O in plane bending, C-C stretching, ...

Tabella A.2: Infrared bands in the spectral region of Amide I, II, III related to the protein secondary structures [32].

Appendice B

Experimental setup

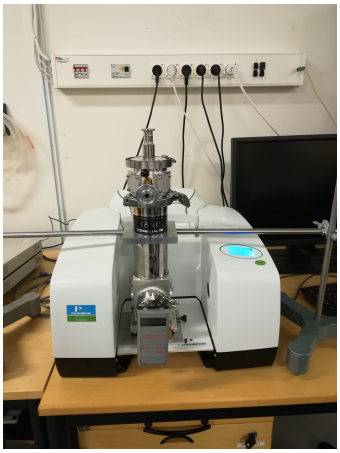

Figura B.1: Fourier transform infrared spectrometer.

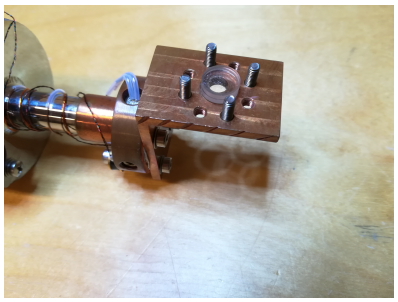

Figura B.2: Cryostat sample holder with dry protein powder sample.

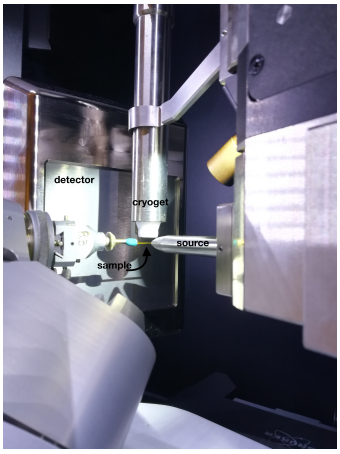

Figura B.3: X-ray diffractometer with the cryoget to cool the sample mounted.

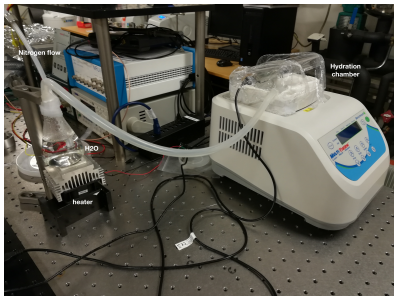

Figura B.4: Hydration setup: nitrogen gas line, water bottle, humidity chamber.

Appendice C

Additional measurements

C.1 Infrared spectra at variable temperature T=160-295 K

Dry Lysozyme powder

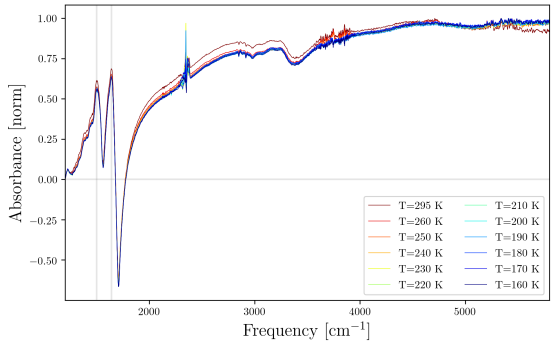

Lysozyme gel

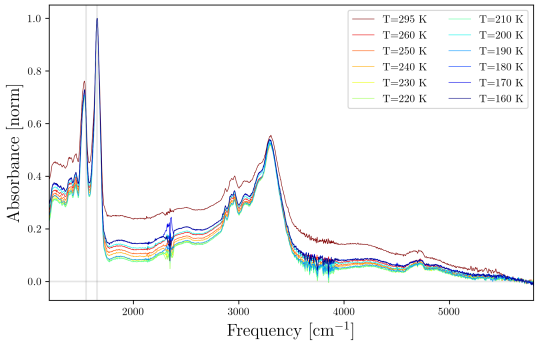

Hydrated lysozyme powder
60 minutes of vapor exposure

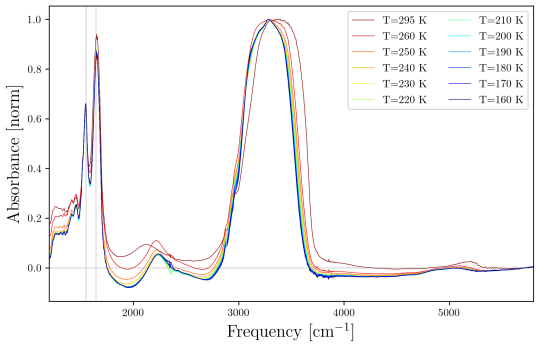

Hydrated lysozyme powder
100 minutes of vapor exposure

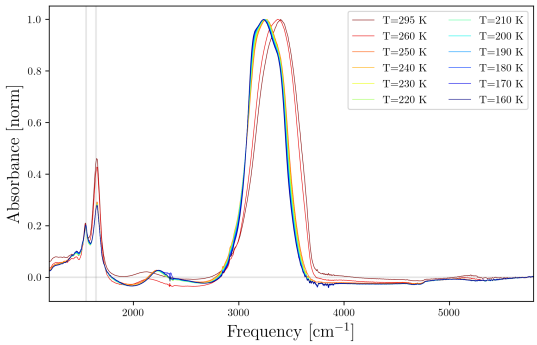

C.2 X-ray diffraction

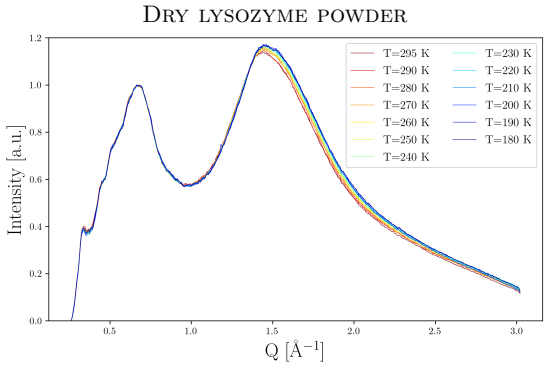

Figura C.1: Angular integrated intensity of dry lysozyme powder at T=180-295 K normalized to the lowest peak.

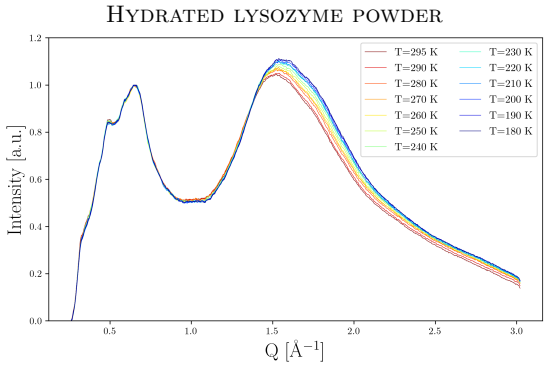

Figura C.2: Angular integrated intensity of dry lysozyme powder at T=180-295 K normalized to the lowest peak.

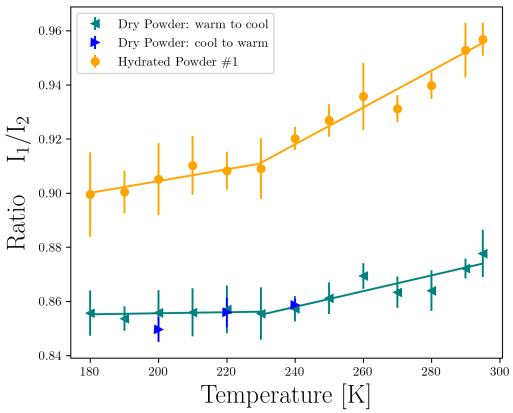

Figura C.3: Ratio of the maxima of $Q\sim 0.62\,Å^{-1}$ and $Q\sim 1.41\,Å^{-1}$ peaks as a function of temperature, for hydrated lysozyme powder (orange dots) and dry lysozyme powder from warm to cool temperatures (teal triangles) and from cool to warm temperatures (blue triangles).

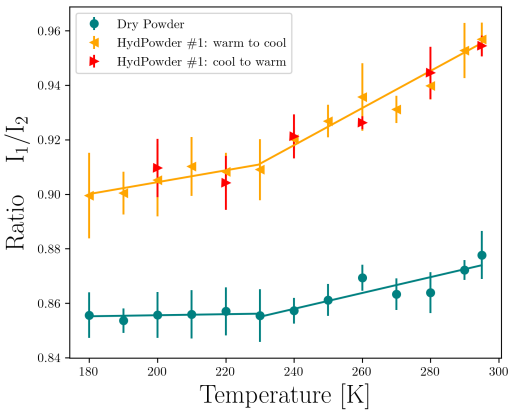

Figura C.4: Ratio of the maxima of $Q\sim 0.62\,Å^{-1}$ and $Q\sim 1.41\,Å^{-1}$ peaks as a function of temperature, for dry lysozyme powder (teal dots) and hydrated lysozyme powder from warm to cool temperatures (orange triangles) and from cool to warm temperatures (red triangles).

Appendice D

Experimental data

Temperature [K]	Ratio I_1/I_2		
	Dry Powder	**Hydrated Powder #1**	**Hydrated Powder #2**
295	0.878 ± 0.009	0.959 ± 0.013	0.957 ± 0.006
290	0.872 ± 0.004	0.950 ± 0.005	0.953 ± 0.010
280	0.864 ± 0.008	0.956 ± 0.005	0.940 ± 0.005
270	0.863 ± 0.006	0.943 ± 0.008	0.931 ± 0.005
260	0.869 ± 0.005	0.946 ± 0.002	0.936 ± 0.012
250	0.861 ± 0.006	0.926 ± 0.006	0.927 ± 0.006
240	0.857 ± 0.005	0.907 ± 0.012	0.920 ± 0.004
230	0.855 ± 0.010	0.912 ± 0.008	0.909 ± 0.011
220	0.857 ± 0.009	0.914 ± 0.005	0.908 ± 0.007
210	0.856 ± 0.009	0.908 ± 0.009	0.910 ± 0.011
200	0.856 ± 0.008	0.910 ± 0.010	0.905 ± 0.013
190	0.854 ± 0.005	0.912 ± 0.004	0.900 ± 0.008
180	0.856 ± 0.008	0.909 ± 0.009	0.899 ± 0.016

Tabella D.1: Ratios of $Q \sim 0.62$ to $Q \sim 1.4$ $\AA^{-1}$ peak intensities, called I_1 and I_2 respectively, for dry lysozyme powder and hydrated lysozyme powder (two different samples prepared under the same experimental conditions). The data are plotted in figure 3.14.

Temperature [K]	Q position	
	Dry Powder [$Å^{-1}$]	Hydrated Powder [$Å^{-1}$]
295	1.412 ± 0.004	1.468 ± 0.002
290	1.416 ± 0.004	1.467 ± 0.002
280	1.415 ± 0.004	1.468 ± 0.003
270	1.424 ± 0.003	1.470 ± 0.002
260	1.420 ± 0.004	1.475 ± 0.002
250	1.424 ± 0.003	1.476 ± 0.003
240	1.427 ± 0.003	1.476 ± 0.002
230	1.426 ± 0.003	1.474 ± 0.002
220	1.418 ± 0.005	1.481 ± 0.003
210	1.428 ± 0.004	1.482 ± 0.003
200	1.427 ± 0.004	1.474 ± 0.003
190	1.428 ± 0.004	1.479 ± 0.004
180	1.428 ± 0.004	1.476 ± 0.003

Tabella D.2: Centers of high-Q peak with its error for dry lysozyme powder (at $Q\sim 1.41\,Å^{-1}$) and hydrated lysozyme powder (at $Q\sim 1.47\,Å^{-1}$). The values are obtained by fitting the peak with a Voigt distribution. The data are plotted in figure 3.15.

Bibliografia

[1] C. A. Angell, *Relaxation in liquids, polymers and plastic crystals - strong/fragile patterns and problems*, Journal of Non-Crystalline Solids, 131-133 (1991), pp. 13–31.

[2] C. A. Angell, *Formation of glasses from liquids and biopolymers*, Science, 267 (1995), pp. 1924–1935.

[3] I. Bahar, R. L. Jernigan, and K. A. Dill, *Protein actions: principles and modeling*, Garland Science, Taylor & Francis Group, 2017.

[4] P. Ball, *H2O: A Biography of Water*, Weidenfeld and Nicolson, Eastbourne, East Sussex, 1999.

[5] H. M. Berman, T. Battistuz, T. N. Bhat, W. F. Bluhm, P. E. Bourne, K. Burkhardt, Z. Feng, G. L. Gilliland, L. Iype, S. Jain, P. Fagan, J. Marvin, D. Padilla, V. Ravichandran, B. Schneider, N. Thanki, H. Weissig, J. Westbrook, and C. Zardecki, *The protein data bank*, Acta Crystallographica Section D: Biological Crystallography, 58 (2002), pp. 899–907.

[6] K. Binder and A. P. Young, *Spin glasses: Experimental facts, theoretical concepts, and open questions*, Reviews of Modern Physics, 58 (1986), pp. 801–976.

[7] J. C. Bischof and X. He, *Thermal stability of proteins*, Annals of the New York Academy of Sciences, 1066 (2006), pp. 12–33.

[8] G. Caliskan, R. M. Briber, D. Thirumalai, V. Garcia-Sakai, S. A. Woodson, and A. P. Sokolov, *Dynamic transition in tRNA is solvent induced*, Journal of the American Chemical Society, 128 (2006), pp. 32–33.

[9] S.-H. Chen, L. Liu, E. Fratini, P. Baglioni, A. Faraone, and E. Mamontov, *Observation of fragile-to-strong dynamic crossover in protein hydration water*, Proceedings of the National Academy of Sciences, 103 (2006), pp. 9012–9016.

[10] L. Cordone, M. Ferrand, E. Vitrano, and G. Zaccai, *Harmonic behavior of trehalose-coated carbon-monoxy-myoglobin at high temperature*, Biophysical Journal, 76 (1999), pp. 1043–1047.

[11] T. E. Creighton, *The biophysical chemistry of nucleic acids*, Helvetian Press, 2011.

[12] A. Cupane and M. Levantino, *Investigating protein structure and dynamics through wide-angle x-ray solution scattering*, Nuovo Cimento, 39 (2016), pp. 1–11.

[13] P. G. Debenedetti, *Supercooled liquids and the glass transition*, Nature, 410 (2001), pp. 259–267.

[14] P. G. Debenedetti, *Supercooled and glassy water*, Journal of Physics: Condensed Matter, 15 (2003), pp. R1669–R1726.

[15] W. Doster, S. Cusack, and W. Petry, *Dynamical transition of myoglobin revealed by inelastic neutron scattering*, Nature, 337 (1989), pp. 754–756.

[16] A. Faraone, L. Liu, C.-Y. Mou, C.-W. Yen, and S.-H. Chen, *Fragile-to-strong liquid transition in deeply supercooled confined water*, The Journal of Chemical Physics, 121 (2004), pp. 10843–10846.

[17] A. Fleming and A. E. Wright, *On a remarkable bacteriolytic element found in tissues and secretions*, Proceedings of the Royal Society of London. Series B, Containing Papers of a Biological Character, 93 (1922), pp. 306–317.

[18] F. Franks, *Water: a matrix of life*, RSC paperbacks, Royal Society of Chemistry, 2nd ed ed., 2000.

[19] H. Frauenfelder, G. Chen, J. Berendzen, P. W. Fenimore, H. Jansson, B. H. McMahon, I. R. Stroe, J. Swenson, and R. D. Young, *A unified model of protein dynamics*, Proceedings of the National Academy of Sciences, 106 (2009), pp. 5129–5134.

[20] H. Frauenfelder, F. Parak, and R. D. Young, *Conformational substates in proteins*, Annual review of biophysics and biophysical chemistry, 17 (1988), pp. 451–479.

[21] H. Frauenfelder, S. G. Sligar, and P. G. Wolynes, *The energy landscapes and motions of proteins*, Science, 254 (1991), pp. 1598–1603.

[22] K. M. Hunter, F. A. Shakib, and F. Paesani, *Disentangling coupling effects in the infrared spectra of liquid water*, The Journal of Physical Chemistry B, 122 (2018), pp. 10754–10761.

[23] J. Jackle, *Models of the glass transition*, Reports on Progress in Physics, 49 (1986), pp. 171–231.

[24] H. Jansson, R. Bergman, and J. Swenson, *Role of solvent for the dynamics and the glass transition of proteins*, The Journal of Physical Chemistry B, 115 (2011), pp. 4099–4109.

[25] K. H. Kim, A. Späh, H. Pathak, F. Perakis, D. Mariedahl, K. Amann-Winkel, J. A. Sellberg, J. H. Lee, S. Kim, J. Park, K. H. Nam, T. Katayama, and A. Nilsson, *Maxima in the thermodynamic response and correlation functions of deeply supercooled water*, Science, 358 (2017), pp. 1589–1593.

[26] C. Kittel, *Introduction to solid state physics*, Wiley, 8th ed ed., 2005.

[27] P. KUMAR, S. V. BULDYREV, AND H. E. STANLEY, *Dynamic crossover and liquid-liquid critical point in the tip5p model of water*, in Soft Matter under Extreme Pressures: Fundamentals and Emerging Technologies, 2006.

[28] P. KUMAR, Z. YAN, L. XU, M. G. MAZZA, S. V. BULDYREV, S.-H. CHEN, S. SASTRY, AND H. E. STANLEY, *Glass transition in biomolecules and the liquid-liquid critical point of water*, Physical Review Letters, 97 (2006), p. 177802.

[29] A. L. LEE AND A. J. WAND, *Microscopic origins of entropy, heat capacity and the glass transition in proteins*, Nature, 411 (2001), pp. 501–504.

[30] R. J. LONCHARICH AND B. R. BROOKS, *Temperature dependence of dynamics of hydrated myoglobin: Comparison of force field calculations with neutron scattering data*, Journal of Molecular Biology, 215 (1990), pp. 439–455.

[31] M. CHAPLIN, *Water structure and science*. `http://www1.lsbu.ac.uk/water/`, 2019. [Online; accessed 17-January-2020].

[32] D. MALLAMACE, E. FAZIO, F. MALLAMACE, AND C. CORSARO, *The role of hydrogen bonding in the folding/unfolding process of hydrated lysozyme: A review of recent NMR and FTIR results*, International Journal of Molecular Sciences, 19 (2018), p. 3825.

[33] F. MALLAMACE, S.-H. CHEN, M. BROCCIO, C. CORSARO, V. CRUPI, D. MAJOLINO, V. VENUTI, P. BAGLIONI, E. FRATINI, C. VANNUCCI, AND H. E. STANLEY, *Role of the solvent in the dynamical transitions of proteins: The case of the lysozyme-water system*, The Journal of Chemical Physics, 127 (2007), p. 045104.

[34] F. MALLAMACE, C. CORSARO, D. MALLAMACE, C. VASI, N. CICERO, AND H. E. STANLEY, *Water and lysozyme: Some results from the bending and stretching vibrational modes*, Frontiers of Physics, 10 (2015), p. 106105.

[35] F. MALLAMACE, C. CORSARO, D. MALLAMACE, S. VASI, C. VASI, AND H. E. STANLEY, *Thermodynamic properties of bulk and confined water*, The Journal of Chemical Physics, 141 (2014), p. 18C504.

[36] Y. MARÉCHAL, *IR spectroscopy of an exceptional h-bonded liquid: water*, Journal of Molecular Structure, 322 (1994), pp. 105–111.

[37] NATIONAL CANCER INSTITUTE, *Cryosurgery in cancer treatment*. `https://www.cancer.gov/about-cancer/treatment/types/surgery/cryosurgery-fact-sheet`, 2005. [Online; accessed 31-January-2020].

[38] A. NILSSON AND L. G. M. PETTERSSON, *The structural origin of anomalous properties of liquid water*, Nature Communications, 6 (2015), p. 8998.

[39] A. NILSSON, S. SCHRECK, F. PERAKIS, AND L. G. M. PETTERSSON, *Probing water with x-ray lasers*, Advances in Physics: X, 1 (2016), pp. 226–245.

[40] S. PAWLUS, S. KHODADADI, AND A. P. SOKOLOV, *Conductivity in hydrated proteins: No signs of the fragile-to-strong crossover*, Physical Review Letters, 100 (2008), p. 108103.

[41] J. T. Pelton and L. R. McLean, *Spectroscopic methods for analysis of protein secondary structure*, Analytical Biochemistry, 277 (2000), pp. 167–176.

[42] F. Perakis, L. De Marco, A. Shalit, F. Tang, Z. R. Kann, T. D. Kühne, R. Torre, M. Bonn, and Y. Nagata, *Vibrational spectroscopy and dynamics of water*, Chemical Reviews, 116 (2016), pp. 7590–7607.

[43] D. C. Phillips, *The hen egg-white lysozyme molecule*, Proceedings of the National Academy of Sciences of the United States of America, 57 (1967), pp. 483–495.

[44] P. H. Poole, F. Sciortino, U. Essmann, and H. E. Stanley, *Phase behaviour of metastable water*, Nature, 360 (1992), pp. 324–328.

[45] M. Praprotnik, D. Janežič, and J. Mavri, *Temperature dependence of water vibrational spectrum: A molecular dynamics simulation study*, The Journal of Physical Chemistry A, 108 (2004), pp. 11056–11062.

[46] B. F. Rasmussen, A. M. Stock, D. Ringe, and G. A. Petsko, *Crystalline ribonuclease a loses function below the dynamical transition at 220 k*, Nature, 357 (1992), pp. 423–424.

[47] D. Ringe and G. A. Petsko, *The 'glass transition' in protein dynamics: what it is, why it occurs, and how to exploit it*, Biophysical Chemistry, 105 (2003), pp. 667–680.

[48] J. A. Rupley and G. Careri, *Protein hydration and function*, in Advances in Protein Chemistry, C. B. Anfinsen, F. M. Richards, J. T. Edsall, and D. S. Eisenberg, eds., vol. 41, Academic Press, 1991, pp. 37–172.

[49] J. A. Sellberg, C. Huang, T. A. McQueen, N. D. Loh, H. Laksmono, D. Schlesinger, R. G. Sierra, D. Nordlund, C. Y. Hampton, D. Starodub, D. P. DePonte, M. Beye, C. Chen, A. V. Martin, A. Barty, K. T. Wikfeldt, T. M. Weiss, C. Caronna, J. Feldkamp, L. B. Skinner, M. M. Seibert, M. Messerschmidt, G. J. Williams, S. Boutet, L. G. M. Pettersson, M. J. Bogan, and A. Nilsson, *Ultrafast x-ray probing of water structure below the homogeneous ice nucleation temperature*, Nature, 510 (2014), pp. 381–384.

[50] R. Shi, J. Russo, and H. Tanaka, *Origin of the emergent fragile-to-strong transition in supercooled water*, Proceedings of the National Academy of Sciences, 115 (2018), pp. 9444–9449.

[51] D. I. Svergun, M. V. Petoukhov, and M. H. J. Koch, *Determination of domain structure of proteins from x-ray solution scattering*, Biophysical Journal, 80 (2001), pp. 2946–2953.

[52] A. M. Tsai, D. A. Neumann, and L. N. Bell, *Molecular dynamics of solid-state lysozyme as affected by glycerol and water: A neutron scattering study*, Biophysical Journal, 79 (2000), pp. 2728–2732.

[53] United Nations, *About the sustainable development goals*. `https://www.un.org/sustainabledevelopment/sustainable-development-goals/`. [Online; accessed 17-January-2020].

[54] M. WEIK, R. B. G. RAVELLI, I. SILMAN, J. L. SUSSMAN, P. GROS, AND J. KROON, *Specific protein dynamics near the solvent glass transition assayed by radiation-induced structural changes*, Protein Science, 10 (2001), pp. 1953–1961.

[55] D. WHITFORD, *Proteins: structure and function*, J. Wiley & Sons, 2005.

[56] R. YOUSIF, *Investigating the influence of water in lysozyme structure and dynamics using FT-IR and XRD*, Stockholm University, 2019.

[57] G. ZACCAI, *How soft is a protein? a protein dynamics force constant measured by neutron scattering*, Science, 288 (2000), pp. 1604–1607.